

A NEW MATHEMATICAL MODEL FOR CELL MOTILITY WITH NONLOCAL REPULSION FROM SATURATED AREAS

CARLO GIAMBIAGI FERRARI, FRANCISCO GUILLÉN-GONZÁLEZ, MAYTE PÉREZ-LLANOS,
AND ANTONIO SUÁREZ

ABSTRACT. The main purpose of this work is the modelling of large populations of cells under different interactions among themselves, in balance with natural random diffusion. We focus on cell-cell adhesion mechanisms for one single population confined in isolated domains. Our most relevant contribution is the proposal of a mathematical model, that includes a nonlocal saturation coefficient multiplying an appropriate nonlocal drift term, that can even induce repulsion effects from saturated areas.

1. INTRODUCTION

Cellular movements are critical for a wide number of biological processes, which go from normal embryogenesis, tissue formation, wound healing and even defense against infection among other. It is also an important factor in diseases such as cancer metastasis and birth defects. Hence, the cellular motion has become an increasingly interesting topic within biomedical research.

It is well known that the cells interact themselves, by attracting and repulsing each other: if they get too close to each other, they repulse, while if they get too far away from each other, they attract. On the other hand, they also exhibit certain random movement. Their natural evolution is a result of the balance between the diffusion originated by the Brownian motion and the transport due to deterministic rules of interaction. When describing their specific interplay, there are delicate aspects to attend, to obtain realistic models. Typically cells move attracted by other cells. However, as an area becomes too crowded with cells, then the attraction they exert to other cells should start to weaken, as far as these other cells tend then to reach less populated areas due to the saturation. This way high accumulations at narrow zones or single points are prevented to occur. How to give form to this effect is far to be simple.

From a mathematical point of view, nonlocal operators are crucial to understand the immense majority of biological processes, by their ability to taking into account the effect of the surrounding environment to describe what happens at certain point, in contrast to local differential operators. One finds a remarkable example in [2], revealing the accuracy of the use of nonlocal models. The drift term moderating cell-cell adhesion has been redefined such that its moving direction is no longer computed differentially, but determined by integral operators. This new nonlocal equation is well posed even for densities whose derivatives reach singular values at certain points. Moreover, the authors stand out the ability of the model to replicate fundamental behaviour associated with cell-cell adhesion and the active sorting process of two or more cell types from a randomly distributed mixture. Paraphrasing the authors, ‘as far as we know no continuous model has previously captured this behaviour’. The relevance of this new nonlocal conception of moving direction inspired a large number of subsequent contributions on the field up to our days. Just a few recent are [7], [9], [10], [12], [13] and [15], etc.

Key words and phrases. Nonlocal gradient, random diffusion, nonlocal saturation coefficient, confined dynamics
2000 *Mathematics Subject Classification* 92C17, 92C37, 35Q92 .

The literature devoted to the use of nonlocal operators, even if we restrict ourselves specifically to cell motion models, is boundless. Far of being exhaustive let us complete the above list referring to the compilation paper on non local cell migration [8] and references therein.

The main concern of this work resides on the description of large populations of cells: how do they evolve in confinement when interacting among them driven by attraction and how do they leave too saturated areas. Moreover, we determine adequate microscopic rules specifically regulating different mechanisms of attraction or repulsion, evaluating the effect of each parameter or term in those relations and the accuracy of the underlying macroscopic behavior.

The content of this paper is organized as follows: We begin by summarizing in Section 2, some existing literature that, indeed, will be the starting point of our work, to be described in the subsequent sections. In Section 3 we propose several discrete models inspired in the references mentioned in Section 2, under the Eulerian perspective. Namely, defining an initial (discrete) density of N cells, we determine its changing rate at every time step, as a balance between loss and gain terms, resulting from the different interactions rules in combination with random motion. This analysis will relate our models as $N \rightarrow \infty$ with certain PDEs containing nonlocal terms. In Section 4 this study will be complemented with a Lagrangian formulation, where we focus on each of the cells motion, according to the mentioned rules. This leads to a system of N ODEs describing each of the cell trajectories. As it should be expected, in the hydrodynamic limit as $N \rightarrow \infty$, this system recovers the same nonlocal PDEs corresponding to the different rules. However, both points of view are meaningful for our purposes. On the one side, Lagrangian perspective allows us to follow every single movement, which is not possible when analyzing a continuous density of cells. On the other side however, the trajectory simulations correspond to a reduced number of particles, thus saturation effects are better described by the PDEs approach. At this point, the discrete Eulerian modelling could be reckon as a numerical discretization of such PDEs, but due to the intricate nature of the problem we use appropriate semi-explicit upwind schemes instead, to obtain reliable results. Several observations for different interactions will be illustrated by a variety of numerical simulations, based on both, Lagrangian trajectories and PDEs discretizations. We conclude the paper enlightening the main conclusions of our analysis in Section 5.

2. PRELIMINARIES AND MAIN OBJECTIVES

In order to understand our analysis, let us briefly review the Armstrong Painter Sherratt model (APS model), see [2], where the density of the population of cells $u(x, t) \geq 0$ in a 1D domain $x \in \Omega$ during a time interval $t \in [0, +\infty)$, evolves according to the nonlocal PDE

$$u_t(x, t) = u_{xx} - \gamma \partial_x \left(u(x, t) K(u)(x, t) \right),$$

being

$$K(u)(x, t) = \int_0^R \left(g(u(x+r, t)) - g(u(x-r, t)) \right) \omega(r) dr.$$

Here $\gamma > 0$ is the strength of the adhesion and $R > 0$ is the sensing radius of a cell. They simplify the model by taking $\omega \equiv 1$ (in their notation a step function), though warn that a non constant function would be more realistic, and also assume one or two dimensional setting and periodic boundary conditions for convenience. As we pointed out in the introduction, the main novelty resides on the proposed drift term $\partial_x(u(x, t)K(u)(x, t))$, where $K(u)$ acts as a nonlocal gradient of the function $g(u)$. When $g(u) = u$, the integral term, $K(u)(x, t)$, is indeed a nonlocal gradient of the density of cells, which drives the cells towards more populated areas, giving raise to strong aggregation in several

peaks, separated $2R$ distance. Further simulations are run in [2] when $g(u) = u(1 - u/k)_+$ is the truncated logistic function by the crowding capacity $k > 0$. This makes that cells travel to medium populated areas, softening the above mentioned peaks. In addition some analysis of several kind of interactions between two populations of different type of cells are investigated, which are out of the scope of this work.

Murakawa and Togashi found in [13] that, when extended to two cell types, the APS model was unable to replicate properly certain cell sorting patterns observed experimentally. Then they propose to replace the linear laplacian diffusion by a porous media diffusion, obtaining a model that captures more accurately the behaviour the authors expected, according to experimental results. Note that even in the simpler case of a single population, this nonlinear diffusion introduces intrinsically a repulsion effect from more crowded areas to empty spaces, stronger than in the Laplacian case, which spreads the particles uniformly along the domain.

However, in [7] Carrillo et al. focus on the drift term, to avoid cells travelling to medium populated areas, as it happens in [13], and instead to be attracted towards the most populated zones. Consequently, they define

$$K(u)(x, t) = (1 - u(x, t)) \int_0^R (u(x + r, t) - u(x - r, t)) \omega(r) dr,$$

where the crowding capacity k has been rescaled, taking the initial data below one. In fact, the variable u of this model can be interpreted as the volume fraction of cells. This model certainly differs from the APS model. On the one hand, even when the cells move to most populated areas through the non local gradient, the velocity of their movement is multiplied by the factor $1 - u(x, t)$, hence this velocity is slower as the area becomes gradually more crowded at x . On the other hand, the nonlinear diffusion of porous media type introduces a repulsion effect to avoid accumulating in high crowded areas.

We notice that repulsion due to saturation is absent in the original APS model, while in [7] and [13] it is driven only by the nonlinear diffusion of porous media type, though not as a result of the drift term. Some remarks in [7] admit that the weight $\omega(r)$ takes positive (aggregation) and negative (repulsion) values, depending on the distance among the interacting cells, but not taking into account the saturation of the area as responsible for such repulsion. In this respect, one of our main interests is to explore the dynamics including repulsion by saturation as part of the drift term. This way we have more control on the influence that each of the different parameters and terms have on the global dynamics, rather than considering a porous media type diffusion to model repulsion from crowded areas.

In addition, in contrast to [7], where the nonlocal gradient is averaged by a piecewise constant weight ω , possibly sign changing, we consider a positive weight, linearly decreasing with respect to the distance within the sensing radius. The profile of each of the aggregations turns out to be more uniformly distributed, than the profile corresponding to a constant weight. In the constant case we observe an unnatural accumulation on the boundaries of each of the formed aggregations, as subsequent histograms show, see Figure 13 below.

Furthermore, the direction of motion will be given by an appropriate coefficient multiplying the nonlocal gradient. One first natural attempt would be modifying the saturation coefficient in [7] so that it changes its sign. For example, taking some $k \in (0, 1)$ and considering $1 - u/k$. However, this coefficient, that only accounts on u at single points, behaves rather unstable. It turns out to be more

proper to define some nonlocal version of the previous coefficient. Namely, choosing $(k - \int_{x-d}^{x+d} u(y)dy)$ for $k \in (0, 1)$ and some small $d > 0$ includes repulsion from saturated areas and enjoys more regularity.

Although [2], [7] and much of the existing literature on mathematical modelling consider periodic boundary conditions, with the consequent simplification of the simulation codes, this approach is just appropriate whenever the size of the domain can be considered infinitely large with respect to cells size. Nevertheless, it is also relevant the study of single-cell migrating in isolation, as it occurs for example when leukocytes migrate during the immune response or when fibroblasts squeeze through connective tissue. Indeed, in [11] it is shown that a polymerizing viscoelastic cytoskeletal gel confined in a narrow channel exhibits spontaneous motion. Interestingly, this mechanism does not require specific adhesion with the channel walls. They prove that there exist cells which are motile only in confined environments while they are unable to move on a flat surface.

Summing up, our main contributions to the previous works are essentially: modelling repulsion from saturated areas with a nonlocal factor multiplying an appropriate nonlocal drift term in isolated domains.

3. EULER PERSPECTIVE

Along this Section we examine various discrete models under the Euler perspective, in the spirit of [14] (see also [1] for biological examples). For simplicity, we assume that the space dimension is $d = 1$ and the domain $\Omega = (-L, L)$. The extension to higher dimensions is straightforward, but would cause high computational cost in the subsequent simulations.

We construct models in which the unknown variable is the proportion of cells at certain position, combining infinitesimal motion directed by a nonlocal signal with random diffusive processes.

3.1. Generic balance. Let $\{1, \dots, N\}$ be the cells, and at time $t = 0$ we assign a real number $x_i(0) \in \bar{\Omega} = [-L, L]$, representing the position of the cell $i \in \{1, \dots, N\}$. The cell's position can only change due to diffusion process and according to different nonlocal interactions between cells inside the sensing radius R . In order to obtain the master equations, let us subdivide the interval $[-L, L]$ in a family of intervals of length h , that is, $\{I_j\}, j \in \{1, \dots, M\}$. Denote as

$$s_j(t) = \frac{\#\{i : x_i(t) \in I_j\}}{N}, \quad j \in \{1, \dots, M\},$$

the proportion of cells with position within the interval I_j , for $j \in \{1, \dots, M\}$. Obviously, $\sum_{j=1}^M s_j(t) = 1$ for all $t \geq 0$.

As in [14], we determine a system of M recursive discrete equations: The proportion of cells at the interval I_j at stage $t + \Delta t$, namely $s_j(t + \Delta t)$, equals to the proportion of cells at I_j in the previous stage, denoted as $s_j(t)$, plus certain gain and loss terms, representing the cells that arrive to I_j at time $t + \Delta t$, and the cells that leave I_j to go somewhere else, under the action of interactions and diffusion. Obviously, the magnitude of these gain and loss terms depend on how long we consider the time step Δt is. At this point we stress an important difference with respect to [14], where Δt was taken such that the proportion of agents (for us cells) at I_j increases or decreases by a factor $1/N$. In our model, the gain and loss terms result from two different effects, interactions and diffusion, which do not occur necessarily with the same frequency. The detailed analysis below shows that indeed, each

of the processes enjoy different scales. Let us fix the characteristic time step Δt . Then,

$$(3.1) \quad s_j(t + \Delta t) = s_j(t) + \Delta t \left[\frac{Q_{\text{diff}}}{N} \left(G_{\text{diff}}(j, t) - L_{\text{diff}}(j, t) \right) + \frac{Q_{\text{int}}}{N} \left(G_{\text{int}}(j, t) - L_{\text{int}}(j, t) \right) \right],$$

where $G_{\text{diff}}(j, t), G_{\text{int}}(j, t)$ stand for probability gain terms while $L_{\text{diff}}(j, t), L_{\text{int}}(j, t)$ represent loss terms, due both to diffusion and interaction effects, respectively. The coefficients Q_{diff} and Q_{int} account for the cardinal of moving cells due to diffusion and interaction processes, respectively, per unit of time.

The key to assemble correctly these two mechanisms of motion, which could combine differential and nonlocal jumps, with local or nonlocal saturation, diffusion, etc., is precisely the determination of the quotient $Q_{\text{int}}/Q_{\text{diff}}$. Note that in some sense, it measures the relative frequency of the interactions occurrence with respect to the diffusion process, revealing the correct scaling of each of the models, so that both effects, interactions and diffusion, play a role in the limit PDE.

The study of the resulting system of M equations (for M large) is easier if considering its continuous version. To this end, we introduce a smooth function representing the probability density of the cell population

$$(3.2) \quad u(x, t) : [-L, L] \times [0, \infty) \rightarrow \mathbb{R}_0^+ \text{ such that } s_j(t) = \int_{I_j} u(x, t) dx \sim h u(x_j, t),$$

being x_j the midpoint of each I_j . In other words, u restricted to the interval I_j behaves as $s_j(t)/h$. With the purpose that $u(x, t)$ also represents the absolute quantity of particles situated on x at time t , it suffices to take $h \sim 1/N$. Indeed, since the number of cells in I_j is

$$N \int_{I_j} u(x, t) dx \sim N h u(x_j, t) \sim u(x_j, t),$$

using in the last approximation that $N h \sim 1$.

From now on we focus on the system of equations (3.1), rewrite it in terms of the continuous density $u(x, t)$ and deduce (formally) different PDEs depending of the model under consideration.

3.2. Diffusive Motion.

Let us precise the gain and loss terms due to the random motion of the cells. Assuming that the jump of the cell is of length h , the proportion of cells arriving to I_j due to diffusion comes from adjacent intervals, with respective probabilities $P_{I_{j+1} \rightarrow I_j} = 1/2 = P_{I_{j-1} \rightarrow I_j}$. Namely,

$$G_{\text{diff}}(t, j) = s_{j+1}(t) P_{I_{j+1} \rightarrow I_j} + s_{j-1}(t) P_{I_{j-1} \rightarrow I_j} = \frac{1}{2} s_{j+1}(t) + \frac{1}{2} s_{j-1}(t).$$

On the other hand, also by diffusion the cells in the interval I_j will leave it to travel to either I_{j-1} or I_{j+1} with respective probabilities $P_{I_j \rightarrow I_{j-1}} = 1/2 = P_{I_j \rightarrow I_{j+1}}$. Thus, the proportion of cells leaving I_j is

$$L_{\text{diff}}(t, j) = s_j(t) (P_{I_j \rightarrow I_{j-1}} + P_{I_j \rightarrow I_{j+1}}) = s_j(t).$$

Consequently, in terms of the density u ,

$$(3.3) \quad \begin{aligned} G_{\text{diff}}(t, j) - L_{\text{diff}}(t, j) &= \frac{1}{2} s_{j+1}(t) + \frac{1}{2} s_{j-1}(t) - s_j(t) \\ &\sim \frac{h}{2} \left[(u(x_{j+1}, t) - u(x_j, t)) + (u(x_{j-1}, t) - u(x_j, t)) \right] \sim \frac{h^3}{2} \Delta u(x_j, t). \end{aligned}$$

3.3. Motion due to aggregation versus repulsion interactions.

Now we turn our attention to the different aggregation-repulsion interaction terms. The total influence acting on a particle is an average of the actions of the rest of population. It is reasonable to assume that in such average the action of cells that are closer to the cell j is stronger than the action exerted by far away cells, which indeed could be even neglected beyond certain threshold, known as the *sensing cell radius* in our context. Then, we assume that interactions are local in space, although the orientation of the cells motion will depend on the cell population in the area within the sensing radius.

3.3.1. Aggregation through nonlocal gradient.

We begin our analysis with the simplest case of the model due to Armstrong, Painter and Sherratt in [2], for which the direction of the transport term is determined by the nonlocal gradient of the density of cells. The action of the surrounding cells decreases linearly with the distance through the weight $w(r)$. This model corresponds to the following gain and loss terms: the proportion of cells arriving to I_j are

$$G_{\text{int}}(t, j) = s_{j+1}(t)P_{I_{j+1} \rightarrow I_j}(t) + s_{j-1}(t)P_{I_{j-1} \rightarrow I_j}(t).$$

The transition probabilities depend now on the configuration of the population inside the sensing zone of cells in I_{j-1} and I_{j+1} , and consequently they are time dependent. Precisely, they are given by

$$P_{I_{j+1} \rightarrow I_j}(t) = \sum_{i=j-r}^j s_i(t)w((j-i)h), \quad P_{I_{j-1} \rightarrow I_j}(t) = \sum_{i=j}^{j+r} s_i(t)w((i-j)h),$$

where again the number r is in fact $r = r(h)$, so that the sensing radius, $R \sim (r(h) + 1)h$, does not depend on h . On the other hand, the proportion of cells leaving I_j are

$$L_{\text{int}}(t, j) = s_j(t) \left[P_{I_j \rightarrow I_{j-1}}(t) + P_{I_j \rightarrow I_{j+1}}(t) \right],$$

being

$$P_{I_j \rightarrow I_{j-1}}(t) = \sum_{i=j-1-r}^{j-1} s_i(t)w((j-1-i)h) \quad P_{I_j \rightarrow I_{j+1}}(t) = \sum_{i=j+1}^{j+1+r} s_i(t)w((i-(j+1))h).$$

With the purpose of identifying the underlying PDE we add and subtract the terms

$$\pm s_j(t)P_{I_{j+1} \rightarrow I_j}(t) \quad \pm s_j(t)P_{I_{j-1} \rightarrow I_j}(t).$$

It yields

$$\begin{aligned} G_{\text{int}}(t, j) - L_{\text{int}}(t, j) &= \left[s_{j+1}(t) - s_j(t) \right] P_{I_{j+1} \rightarrow I_j}(t) + \left[s_{j-1}(t) - s_j(t) \right] P_{I_{j-1} \rightarrow I_j}(t) \\ &\quad + s_j(t) \left[P_{I_{j+1} \rightarrow I_j}(t) - P_{I_j \rightarrow I_{j-1}}(t) \right] + s_j(t) \left[P_{I_{j-1} \rightarrow I_j}(t) - P_{I_j \rightarrow I_{j+1}}(t) \right] \\ &:= T1 + T2 + T3 + T4. \end{aligned}$$

Observe that, using the equality

$$(3.4) \quad (a_{j+1} - a_j)b_{j+1} - a_j(b_{j+1} - b_j) = a_{j+1}b_{j+1} - a_jb_j,$$

one has

$$\begin{aligned} T1 + T3 &= s_{j+1}(t)P_{I_{j+1} \rightarrow I_j}(t) - s_j(t)P_{I_j \rightarrow I_{j-1}}, \\ T2 + T4 &= s_{j-1}(t)P_{I_{j-1} \rightarrow I_j}(t) - s_j(t)P_{I_j \rightarrow I_{j+1}}. \end{aligned}$$

Taking into account that

$$\begin{aligned} P_{I_{j+1} \rightarrow I_j}(t) &= \sum_{i=j-r}^j s_i(t) w((j-i)h) \\ &\sim \sum_{i=j-r}^j h u(x_i, t) w((j-i)h) \sim \int_{x_j-R}^{x_j} u(y, t) w(x_j - y) dy \end{aligned}$$

and similarly

$$P_{I_{j-1} \rightarrow I_j}(t) \sim \int_{x_j}^{x_j+R} u(y, t) w(y - x_j) dy,$$

one arrives at

$$\begin{aligned} T1 + T3 &\sim h^2 \frac{\partial}{\partial x} \left(u(x_j, t) \int_{x_{j-1}-R}^{x_{j-1}} u(y, t) w(x_{j-1} - y) dy \right), \\ T2 + T4 &\sim -h^2 \frac{\partial}{\partial x} \left(u(x_j, t) \int_{x_{j+1}}^{x_{j+1}+R} u(y, t) w(y - x_{j+1}) dy \right). \end{aligned}$$

Summing up

$$(3.5) \quad G_{\text{int}}(t, j) - L_{\text{int}}(t, j) \sim -h^2 \frac{\partial}{\partial x} \left(u(x_j, t) (\nabla_{NL} u)(x_j, t) \right),$$

being the nonlocal gradient defined as

$$(3.6) \quad (\nabla_{NL} u)(x_j, t) = \int_{x_{j+1}}^{x_{j+1}+R} u(y, t) w(y - x_{j+1}) dy - \int_{x_{j-1}-R}^{x_{j-1}} u(y, t) w(x_{j-1} - y) dy.$$

We notice that in [2] it is also proposed to consider as drift term the nonlocal gradient of the truncated logistic function $g(u) = u(1-u)_+$, which avoids the strong aggregation exhibited by the previous model. However, this choice does not fit the point of view of our modeling. Furthermore, in [7] it is discussed the appropriateness of this specific logistic drift term. Among other reasons, the authors in [7] do not agree with the fact that cells are attracted by medium populated areas. Accordingly, to soften the strong aggregation they propose instead, to include a coefficient of saturation in the APS model with $g(u) = u$. Inspired in this proposal, we derive the following discrete model that reproduces the dynamics in [7].

3.3.2. Aggregation through nonlocal gradient with local coefficient of saturation.

We notice that in [7] the variable $u(x, t)$ is regarded to be bounded by one, representing the proportion of cells at position x at time t . Therefore, we do not consider the continuous approach given by our function u in (3.2). Instead, we take a continuous function approaching the proportion (or volume fraction) variable, \hat{u} , such that

$$\frac{1}{h} \int_{I_j} \hat{u}(x, t) dx = s_j(t).$$

As before,

$$G_{\text{int}}(t, j) - L_{\text{int}}(t, j) = s_{j+1}(t) P_{I_{j+1} \rightarrow I_j}(t) - s_j(t) P_{I_j \rightarrow I_{j-1}} + s_{j-1}(t) P_{I_{j-1} \rightarrow I_j}(t) - s_j(t) P_{I_j \rightarrow I_{j+1}}.$$

Moreover, in [7] the transition probabilities are modeled now by a saturation coefficient $(1 - s_j(t))$ for each cell positioned at I_j

$$P_{I_{j+1} \rightarrow I_j}(t) = (1 - s_{j+1}(t)) \sum_{i=j-r}^j s_i(t) w((j-i)h)$$

$$P_{I_{j-1} \rightarrow I_j}(t) = (1 - s_{j-1}(t)) \sum_{i=j}^{j+r} s_i(t) w((i-j)h).$$

Arguing as in the previous case the following approximation is deduced

$$(3.7) \quad G_{\text{int}}(t, j) - L_{\text{int}}(t, j) \sim -\frac{\partial}{\partial x} \left(\hat{u}(x_j, t) (1 - \hat{u}(x_j, t)) (\nabla_{NL} \hat{u})(x_j, t) \right),$$

where the nonlocal gradient ∇_{NL} is given in (3.6). Notice the difference of scale with respect to the strong aggregation model and the point-wise estimate $0 \leq \hat{u}(x, t) \leq 1$.

3.3.3. Aggregation/repulsion through nonlocal gradient with nonlocal coefficient of saturation.

One of our main objectives is to include the effect of repulsion as part of the cells interaction. With this aim in mind, in the transition probabilities let us consider now a nonlocal saturation coefficient for cells positioned at x_j :

$$(3.8) \quad K - \sum_{i=j-l}^{j+l} s_i(t).$$

Here, the parameter $K \in (0, 1)$ represents a threshold for the crowding capacity of nonlocal type in the interval $[x_j - lh, x_j + lh] \cap [-L, L]$ for each $x_j \in [-L, L]$. As before $l = l(h)$, so that in the limit the saturation radius $[x_j - lh, x_j + lh] = [x_j - R_{sat}, x_j + R_{sat}]$ is independent of h . In (3.8) we could also ponder the influence of neighboring cells through a non-constant weight $\hat{\omega}$, namely

$$K - \sum_{i=j-l}^{j+l} s_i(t) \hat{\omega}((j-i)h).$$

By simplicity we take $\hat{\omega} \equiv 1$. Indeed, subsequent simulations in Section 4.1 show that taking a linear weight $\hat{\omega}$ does not differ substantially from the dynamics with $\hat{\omega} \equiv 1$, specially when R_{sat} is small. Compare for example first picture in Figure 12 (where $\hat{\omega} \equiv 1$) with third picture of Figure 15 (with $\hat{\omega}(y) = (R_{sat} - y)/R_{sat}$).

The nonlocal coefficient (3.8) acts on the motion of the cells as follows: a cell positioned at certain x_j moves accordingly aggregation influences whenever the amount of cells around its position does not exceed the crowding capacity K . Above this threshold, the cell begins to move towards less populated areas as a result of repulsion. This has to be contrasted with respect to the previous model, where cells at populated positions merely slow down their velocity of displacement, saturating those areas. One could think that a simpler way to extend the previous model to exhibit repulsion could consist on changing the factor $(1 - s_j(t))$ by $(K - s_j(t))$ for $K < 1$. Indeed we obtain repulsion effects. However, since we are measuring the proportion of cells at a single position, the dynamics becomes highly oscillating when passing to the limit as $h \rightarrow 0$. In the next section we have depicted cell trajectories corresponding to this coefficient, where this instability can be easily observed in Figure 11. The coefficient (3.8) smooths these high oscillations and produces a more realistic model, see Figures 12 and 13.

As before, cells arriving to I_j and starting from I_j are given by the gain-loss term:

$$G_{\text{int}}(t, j) - L_{\text{int}}(t, j) = s_{j+1}(t)P_{I_{j+1} \rightarrow I_j}(t) - s_j(t)P_{I_j \rightarrow I_{j-1}} + s_{j-1}(t)P_{I_{j-1} \rightarrow I_j}(t) - s_j(t)P_{I_j \rightarrow I_{j+1}}$$

where the transition probabilities are driven now by two effects. Cells moving from I_{j+1} towards I_j (resp. from I_{j-1} towards I_j) respond to two processes: aggregation produced by cells at left hand side inside the sensing radius (resp. at right hand side) and saturation produced by the existing cells at right hand side (resp. at left hand side). Precisely, denoting as $(g)_- = \min\{g, 0\}$ and $(g)_+ = \max\{g, 0\}$, we will split the nonlocal saturation coefficient (3.8) into its positive and negative parts as follows

$$\begin{aligned} P_{I_{j+1} \rightarrow I_j}(t) &= - \left(K - \sum_{i=j+1-l}^{j+1+l} s_i(t) \right)_- \sum_{i=j+2}^{j+2+r} s_i(t) w((i - (j+2))h) \quad (\text{repulsion term}) \\ &\quad + \left(K - \sum_{i=j+1-l}^{j+l} s_i(t) \right)_+ \sum_{i=j-r}^j s_i(t) w((j-i)h) \quad (\text{aggregation term}) \\ P_{I_{j-1} \rightarrow I_j}(t) &= - \left(K - \sum_{i=j-1-l}^{j-1+l} s_i(t) \right)_- \sum_{i=j-2-r}^{j-2} s_i(t) w((j-2-i)h) \quad (\text{repulsion term}) \\ &\quad + \left(K - \sum_{i=j-1-l}^{j-1+l} s_i(t) \right)_+ \sum_{i=j}^{j+r} s_i(t) w((i-j)h) \quad (\text{aggregation term}). \end{aligned}$$

Now we proceed with the translation of the above terms into a continuous setting. For example, with the terms $P_{I_{j+1} \rightarrow I_j}(t)_{(1)} - P_{I_j \rightarrow I_{j-1}}(t)_{(1)}$, corresponding to gain and loss terms by repulsion effects, we

act as follows

$$\begin{aligned}
& s_{j+1}(t)P_{I_{j+1} \rightarrow I_j}(t)_{(1)} - s_j(t)P_{I_j \rightarrow I_{j-1}}(t)_{(1)} \\
&= s_{j+1}(t)P_{I_{j+1} \rightarrow I_j}(t)_{(1)} + s_j(t) \left(K - \sum_{i=j-l}^{j+l} s_i(t) \right) \sum_{i=j+2}^{j+2+r} s_i(t)w((i-(j+2))h) \\
&\quad - s_j(t)P_{I_j \rightarrow I_{j-1}}(t)_{(1)} - s_j(t) \left(K - \sum_{i=j-l}^{j+l} s_i(t) \right) \sum_{i=j+2}^{j+2+r} s_i(t)w((i-(j+2))h) \\
&= - \left[s_{j+1}(t) \left(K - \sum_{i=j+1-l}^{j+1+l} s_i(t) \right) - s_j(t) \left(K - \sum_{i=j-l}^{j+l} s_i(t) \right) \right] \sum_{i=j+2}^{j+2+r} s_i(t)w((i-(j+2))h) \\
&\quad - s_j(t) \left(K - \sum_{i=j-l}^{j+l} s_i(t) \right) \left[\sum_{i=j+2}^{j+2+r} s_i(t)w((i-(j+2))h) - \sum_{i=j+1}^{j+1+r} s_i(t)w((i-(j+1))h) \right] \\
&= -h u(x_{j+1}, t) \left(K - \sum_{i=j+1-l}^{j+1+l} s_i(t) \right) \sum_{i=j+2}^{j+2+r} h u(x_i, t)w((i-(j+2))h) \\
&\quad + h u(x_j, t) \left(K - \sum_{i=j-l}^{j+l} s_i(t) \right) \sum_{i=j+1}^{j+1+r} h u(x_i, t)w((i-(j+1))h) \\
&\sim -h^2 \frac{\partial}{\partial x} \left(u(x_j, t) \left(K - \int_{x_j-R_{sat}}^{x_j+R_{sat}} u(y, t)dy \right) - \int_{x_{j+1}}^{x_{j+1}+R} u(y, t)w(y-x_{j+1})dy \right),
\end{aligned}$$

where in the last equality the formula (3.4) is used. Similar arguments with the rest of the terms yield to

$$(3.9) \quad G_{\text{int}}(t, j) - L_{\text{int}}(t, j) \sim -h^2 \frac{\partial}{\partial x} \left(u(x_j, t) \left(K - \int_{x_j-R_{sat}}^{x_j+R_{sat}} u(y, t)dy \right) \nabla_{NL} u(x_j, t) \right),$$

where $\nabla_{NL} u$ is specified in (3.6).

3.3.4. Boundary effects.

In the above descriptions of gain and loss terms we have not taken into account the effects of the boundary, writing the formulae for intervals very far from it, for simplicity. For intervals closer to the boundary we consider isolating conditions. Namely, any arriving particle belongs to the domain and on the other hand, the particles cannot leave this domain. We anticipate that this assumption will yield Robin type boundary conditions, 3.11 in the continuous case. However, in practice we consider the particular case of double isolation to simplify the simulations. This means that the limit density u satisfies homogeneous Neumann boundary conditions. At the same time, motion corresponding to aggregation/repulsion is also restricted to the interior of the domain. Both assumptions are represented through condition 3.15. If capacity is large, cells at the boundary are more likely to be pushed towards the interior by the attraction of other cells, while from outside they do not experiment neither attraction nor repulsion, see for instance Figure 3. Under strong repulsion the scenery is completely different: cells could be pushed towards the boundary, where they could form high accumulations peaks due to isolation, see Figure 4. Moreover, constant initial conditions immediately start their dynamics

exclusively as a result of the isolated conditions, without need of being perturbed, as it happens with periodic boundary conditions.

3.4. Dynamics driven by the interplay between diffusion and nonlocal drift terms.

We study now the combined effect of random diffusion, combined with different aggregation/repulsion effects and derive the corresponding PDEs.

3.4.1. Super aggregation [2].

Let us assume that the drift term follows the APS model. Then, relating (3.1), (3.3) and (3.5) we obtain

$$h \frac{u(x_j, t + \Delta t) - u(x_j, t)}{\Delta t} \sim \frac{h^3}{2} \frac{Q_{\text{diff}}}{N} \Delta u(x_j, t) - \frac{Q_{\text{int}}}{N} h^2 \frac{\partial}{\partial x} \left(u(x_j, t) (\nabla_{NL} u)(x_j, t) \right),$$

with $(\nabla_{NL} u)$ specified in (3.6).

Then taking

$$\frac{Q_{\text{int}}}{Q_{\text{diff}}} \sim \frac{1}{2} h \gamma,$$

with $\gamma > 0$ a parameter related to the interactions strength, and after appropriate time scaling it yields the following nonlocal PDE for a generic $x \in (-L, L)$

$$(3.10) \quad u_t(x, t) = \Delta u(x, t) - \gamma \frac{\partial}{\partial x} \left(u(x, t) (\nabla_{NL} u)(x, t) \right),$$

and boundary conditions

$$(3.11) \quad u_x(L, t) + \gamma u(L, t) \int_0^R u(L - r, t) w(r) dr = 0 \quad \text{and} \quad u_x(-L, t) - \gamma u(-L, t) \int_0^R u(-L + r, t) w(r) dr = 0.$$

Here,

$$(3.12) \quad (\nabla_{NL} u)(x, t) = \int_x^{x+R} u(y, t) w(y - x) \mathbb{1}_{\overline{\Omega}}(y) dy - \int_{x-R}^x u(y, t) w(x - y) \mathbb{1}_{\overline{\Omega}}(y) dy$$

where the characteristic function $\mathbb{1}_{\overline{\Omega}}$ acts in the integrals on the points x whose distance to the boundary is less than the sensing radius R .

3.4.2. Local saturation [7].

We are assuming now that the gain and loss terms due to interactions are given by (3.7). The gain and loss terms due to random diffusion for \hat{u} in (3.3) take the form

$$G_{\text{diff}}(t, j) - L_{\text{diff}}(t, j) \sim \frac{h^2}{2} \Delta \hat{u}(x_j, t).$$

Then (3.1) reads as

$$\frac{\hat{u}(x_j, t + \Delta t) - \hat{u}(x_j, t)}{\Delta t} \sim \frac{h^2}{2} \frac{Q_{\text{diff}}}{N} \Delta \hat{u}(x_j, t) - \frac{Q_{\text{int}}}{N} \frac{\partial}{\partial x} \left(\hat{u}(x_j, t) (1 - \hat{u}(x_j, t)) (\nabla_{NL} \hat{u})(x_j, t) \right),$$

where the nonlocal gradient ∇_{NL} is defined in (3.6). Choosing

$$\frac{Q_{\text{int}}}{Q_{\text{diff}}} \sim \frac{1}{2} h^2 \gamma,$$

rescaling the time accordingly and passing to the limit, we arrives at the nonlocal PDE

$$(3.13) \quad \hat{u}_t(x, t) = \Delta \hat{u}(x, t) - \gamma \frac{\partial}{\partial x} \left(\hat{u}(x, t) (1 - \hat{u}(x, t)) (\nabla_{NL} \hat{u})(x, t) \right),$$

with $\nabla_{NL}\hat{u}$ given by (3.12) and similar boundary conditions as in (3.11), just replacing in the interaction term, the coefficient γu by $\gamma\hat{u}(1-\hat{u})$. Notice that in this case $0 \leq \hat{u} \leq 1$.

3.4.3. A new nonlocal aggregation/repulsion model.

Replacing the saturation coefficient by (3.8), and using again (3.3) and (3.9), the PDE (3.1) reads now

$$h \frac{u(x_j, t + \Delta t) - u(x_j, t)}{\Delta t} \sim \frac{h^3}{2} \frac{Q_{\text{diff}}}{N} \Delta u(x_j, t) - h^2 \frac{Q_{\text{int}}}{N} \frac{\partial}{\partial x} \left(u(x_j, t) \left(K - \int_{x_j - R_{\text{sat}}}^{x_j + R_{\text{sat}}} u(y, t) dy \right) \nabla_{NL} u(x_j, t) \right).$$

See (3.6) for the definition of the interaction term. Thus taking

$$\frac{Q_{\text{int}}}{Q_{\text{diff}}} \sim \frac{1}{2} h \gamma,$$

and rescaling the time, it gives the nonlocal PDE

$$(3.14) \quad u_t(x, t) = \Delta u(x, t) - \gamma \frac{\partial}{\partial x} \left(u(x, t) \left(K - \int_{x - R_{\text{sat}}}^{x + R_{\text{sat}}} u(y, t) \mathbb{1}_{\bar{\Omega}}(y) dy \right) \nabla_{NL} u(x, t) \right),$$

with similar boundary conditions as in (3.11), just replacing in the interaction term, u by $u(K - \int_{x - R_{\text{sat}}}^{x + R_{\text{sat}}} u(y, t) \mathbb{1}_{\bar{\Omega}}(y) dy)$.

3.5. Numerical simulations.

We conclude this section performing some numerical simulations. We focus on the new model proposed in Section 3.3.3, to illustrate how the different effects (sensing and saturation radius, nonlocal capacity, etc.) act on the spontaneous random movements of the cells, comparing the corresponding asymptotic patterns obtained for each case.

Notice that the general equation (3.1) could be thought as a simple explicit Euler time scheme, and the subsequence identification of the diffusion and interactions terms as a centered Finite Difference in space scheme, of the resulting PDE. However, since we wish to describe the final distribution of cells under the balance of all of the actions, an explicit and centered numerical method is not appropriate. Under the interaction dominance, strong aggregation and repulsion could eventually destabilize the numerical results approximating (3.14). To tackle with this difficulty we propose an implicit linear scheme in time to approach (3.14) and upwind Finite Volume schemes (of Godunov type) in space, a well known technique widely used when simulating propagating phenomena. Roughly speaking, upwind schemes attempt to discretize the equation by using differences biased in the direction determined by the sign of the characteristic speeds. Thanks to the sparse structure of both, diffusion and interaction matrices, an implicit centered approximation scheme results a very robust and efficient numerical approach.

Regarding the boundary conditions, we have imposed the dynamics to remain doubly isolated, which means splitting condition (3.11) into

$$(3.15) \quad u_x(L, t) = 0, \int_0^R u(L - r, t) w(r) dr = 0 \quad \text{and} \quad u_x(-L, t) = 0, \int_0^R u(-L + r, t) w(r) dr = 0.$$

These turn out to be as well the boundary conditions for the three models studied here, including a local saturation and nonlocal repulsion/aggregation coefficient, with double isolation, for an easier implementation. All of the subsequent simulations are performed in the interval $\bar{\Omega} = [-1, 1]$ with a uniform spatial mesh of size $h = 2 \cdot 10^{-4}$. The suitable time scale however, depends of the example

under consideration, to capture appropriately the intermediate states and understand the dynamics as a result of the balance among all of the mechanisms. In this sense it is also essential to calibrate the intensity of the interactions, represented by the coefficient γ . In most of the examples will take the value $\gamma = 10^5$ in order to detect the two different effects, diffusion and interaction, involved in the equation.

In the following simulations, we depict the evolution of a single asymmetric cells density, being initially $u_0(x) = (x+1)^2(1-x)^2(1+\sin(\pi x))$ given in Figure 1, under repulsion and aggregation forces according to model 3.14, with different intensities. We also vary the parameters delimiting the non-locality of the different effects: R the sensing radius and R_{sat} the saturation radius.

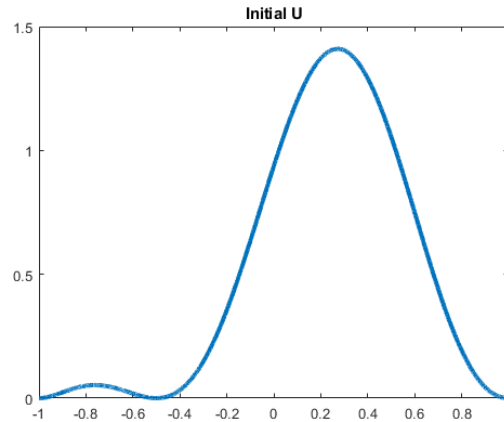


FIGURE 1. Initial condition $u_0(x) = (x+1)^2(1-x)^2(1+\sin(\pi x))$

Our first example in Figure 2, considers an intermediate repulsion. Specifically, the nonlocal capacity with value $K = 0.6$ and equilibrated nonlocal radius parameters $R = R_{sat} = 0.2$. We can observe that, once the main accumulation has split into two accused peaks due to repulsion, the roles of motion are undertaken mostly by aggregation and diffusion, except for the interval $[0.1, 0.5]$, approximately. Here, repulsion exerted by the accumulation peaks still acts, as can be appreciated in the fourth picture of Figure 2. The profile eventually equilibrate, as a result of the balance of the quantity of cells. Notice the zoom we include in the first picture of the second line of Figure 2. This small density of cells between both peaks equilibrates both sides of the nonlocal gradient. In fact, last picture shows the values of the nonlocal gradient at this final stage, which are very close to zero, hence the future motion of the cells is almost imperceptible. Cells on the left hand side of the first aggregation peak still move to the right, attracted by the accumulation, though extremely slow. In the same way, the particles situated on the right hand side move towards left, attracted by the second peak. But note that precisely within the area where repulsion takes place, the values of the nonlocal flux are even closer to zero.

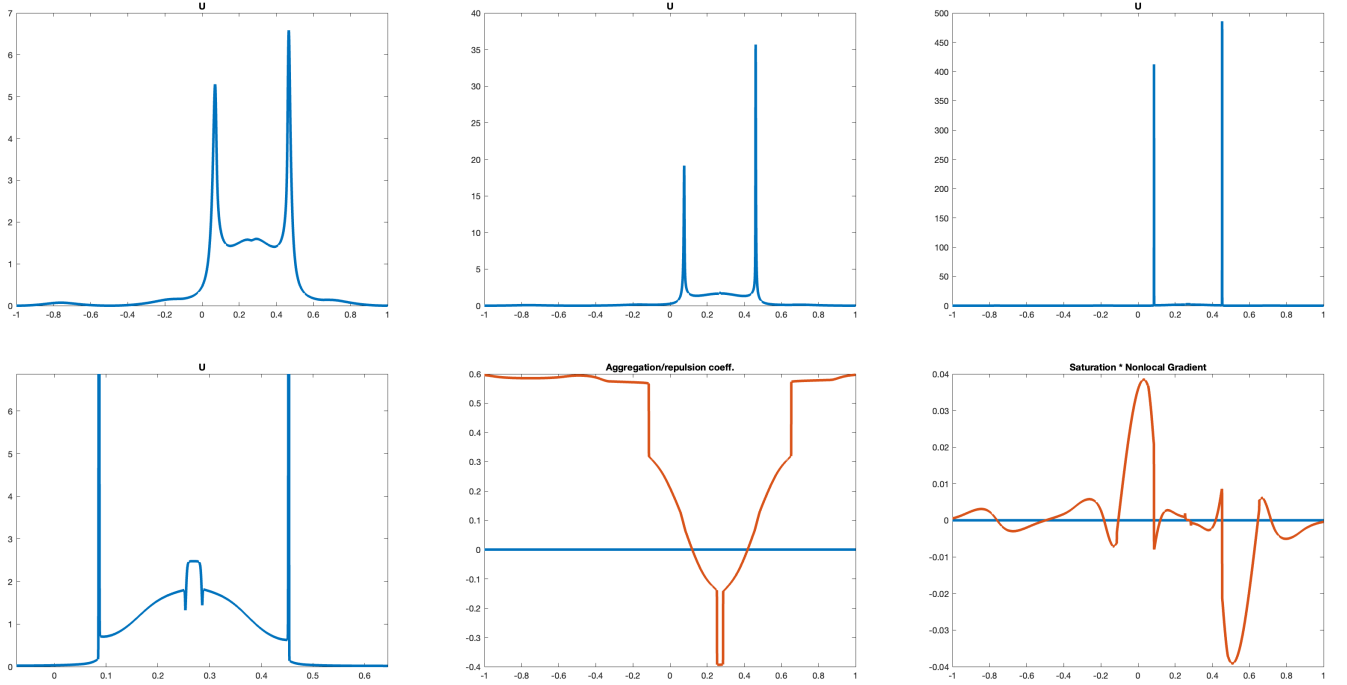


FIGURE 2. Evolution of a cell population under equilibrated nonlocal parameters $R = R_{sat} = 0.2$ governed by a weak repulsion $K = 0.6$. The first line of pictures corresponds to the evolution of the density of cells at different times. In the line below we represent a zoom of the final profile at the area between the two strong aggregations. We also depict the aggregation/repulsion coefficient and the nonlocal flux corresponding to this final state.

If in the above model we increase the repulsion up to $K = 0.2$, then we can observe a completely different profile, see Figure 3. It is quite noticeable the effect driven by the double isolated boundary conditions. Even when there is a strong aggregation close to $x = 1$ the profile reaches the boundary with null slope. Again, the final profile remains stable after a redistribution of the density that reduces drastically the flux values, being of order 10^{-3} , yielding almost imperceptible motion.

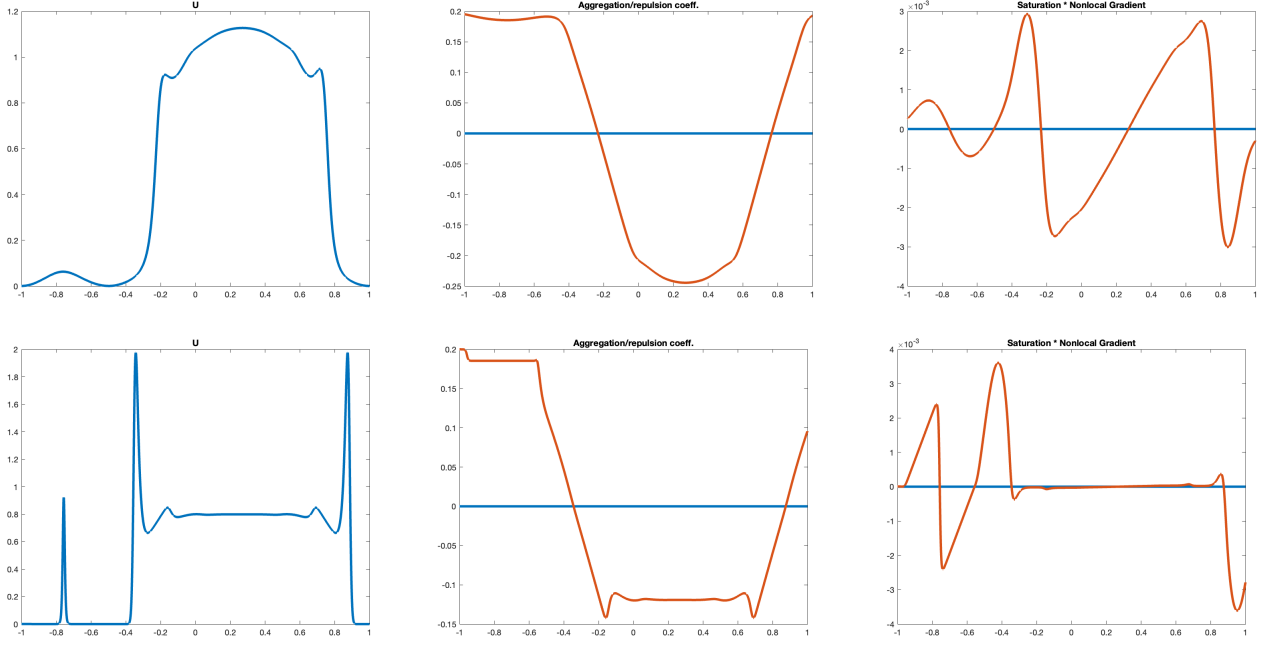


FIGURE 3. Evolution of a cell population under equilibrated nonlocal parameters $R = R_{sat} = 0.2$ governed by strong repulsion ($K = 0.2$). We depict the cell density profile, the aggregation/repulsion coefficient, and the drift term, at certain intermediate time (first line), and at the final time (second line).

Keeping the same parameters of Figures 2 and 3, we strength the capacity coefficient upto $K = 0.1$, obtaining as a result a strong repulsive motion. We specially remark the different behaviour with respect to the case $K = 0.2$ in Figure 3. Notice that now both accumulation peaks lay exactly on the boundaries, where the cells remain stunk as a result of the boundary isolating assumptions. Despite of the homogeneous Neumann boundary conditions for the diffusive motion, it is the drift term boundary condition that prevails under strong repulsion dynamics.

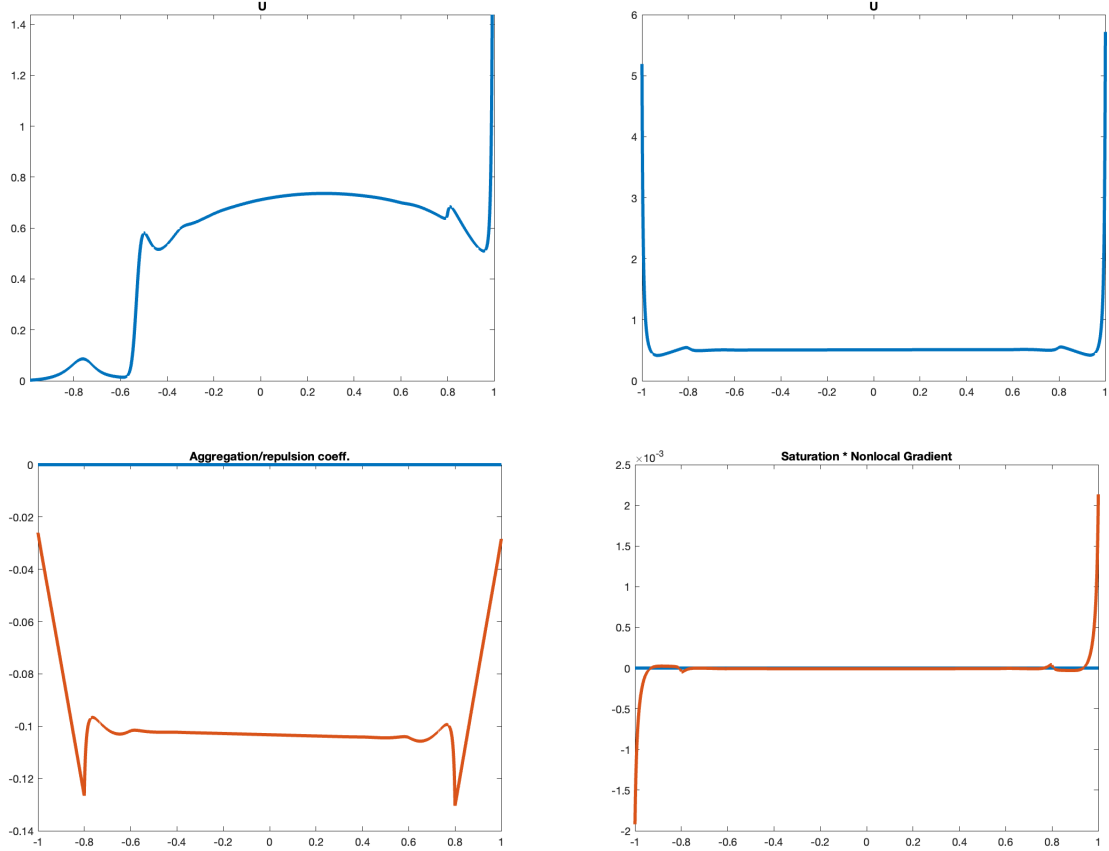


FIGURE 4. Evolution of a cell population under equilibrated nonlocal parameters $R = R_{sat} = 0.2$ governed by very strong repulsion ($K = 0.1$). We depict the cell distribution profile at an intermediate stage and at the final state on the first line. On the second line we include the aggregation/repulsion coefficient and the drift term at the equilibrium.

We conclude the observations of this example analyzing the remaining case of very strong aggregation, that is, the nonlocal capacity being highly close to one. We begin by taking $K = 0.8$, which allows that several aggregation peaks arise more or less periodically separated 0.3 units on the right hand side of the interval. However, there are remaining cells between the main peaks as it can be observed in the amplified zoom in the second picture of Figure 5. In particular, on the peak situated on $[0.2, 0.35]$ a weak repulsion acts driving cells to both surrounding peaks, while in the rest of the interval, cells move as response only to aggregation process. Indeed, the picture of the nonlocal flux matches with the aggregation action: cells move towards the peaks. However, within the repulsion area there is not movement.

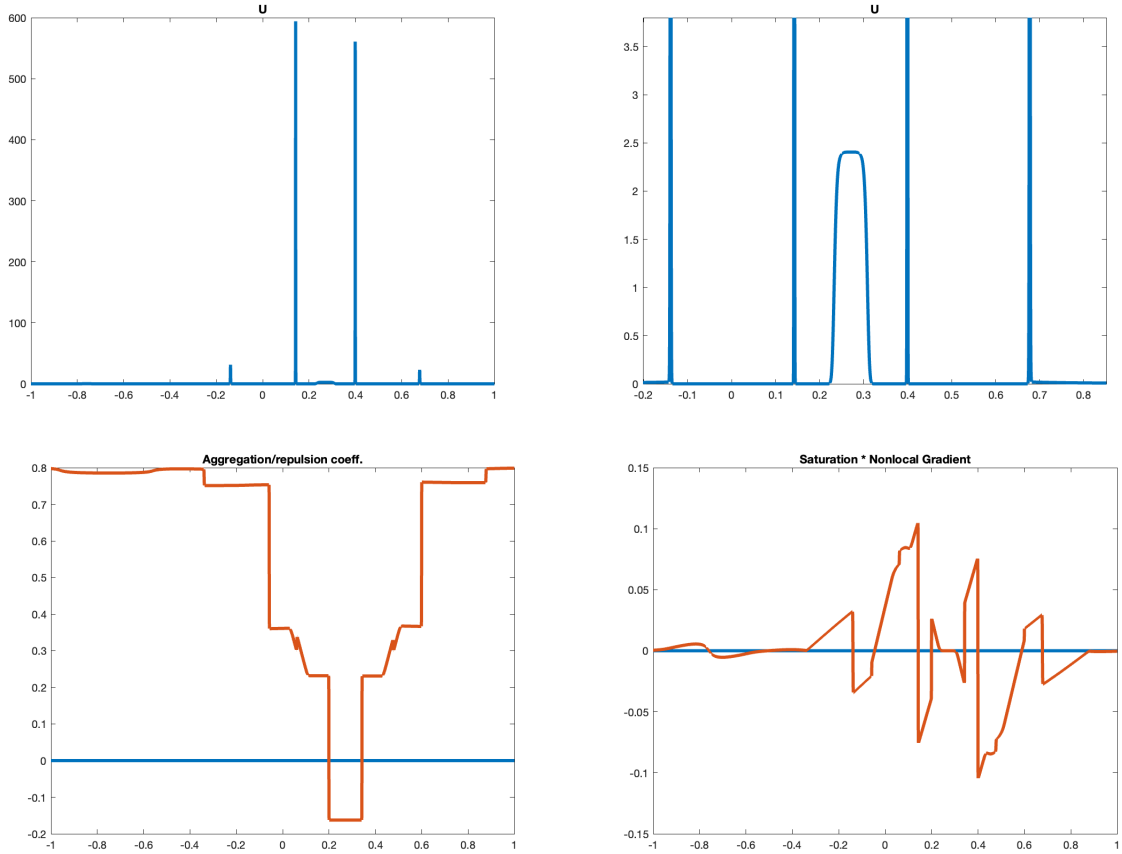


FIGURE 5. Evolution of a cell population under equilibrated nonlocal parameters $R = R_{sat} = 0.2$ governed by strong aggregation ($K = 0.8$). On the first line we represent the cell distribution profile at equilibrium and zoom of the accumulation area between the main two peaks. The second line contains the final stage of the aggregation/repulsion coefficient and flux.

Finally, if $K = 0.95$ even when the final profile is quite similar to the previous case, an analysis of the drift term coefficient shows that repulsion has totally lost any role in the dynamics, even in the interval $[0.2, 0.4]$, see Figure 6. Moreover, any of those strong accumulations produces stronger attraction than the population situated approximately on the interval $[0.18, 0.38]$, where the interaction coefficient attains minimum values. Furthermore, the gradient is almost null in this interval. Accordingly, we can appreciate a not vanishing density in this interval at the equilibria.

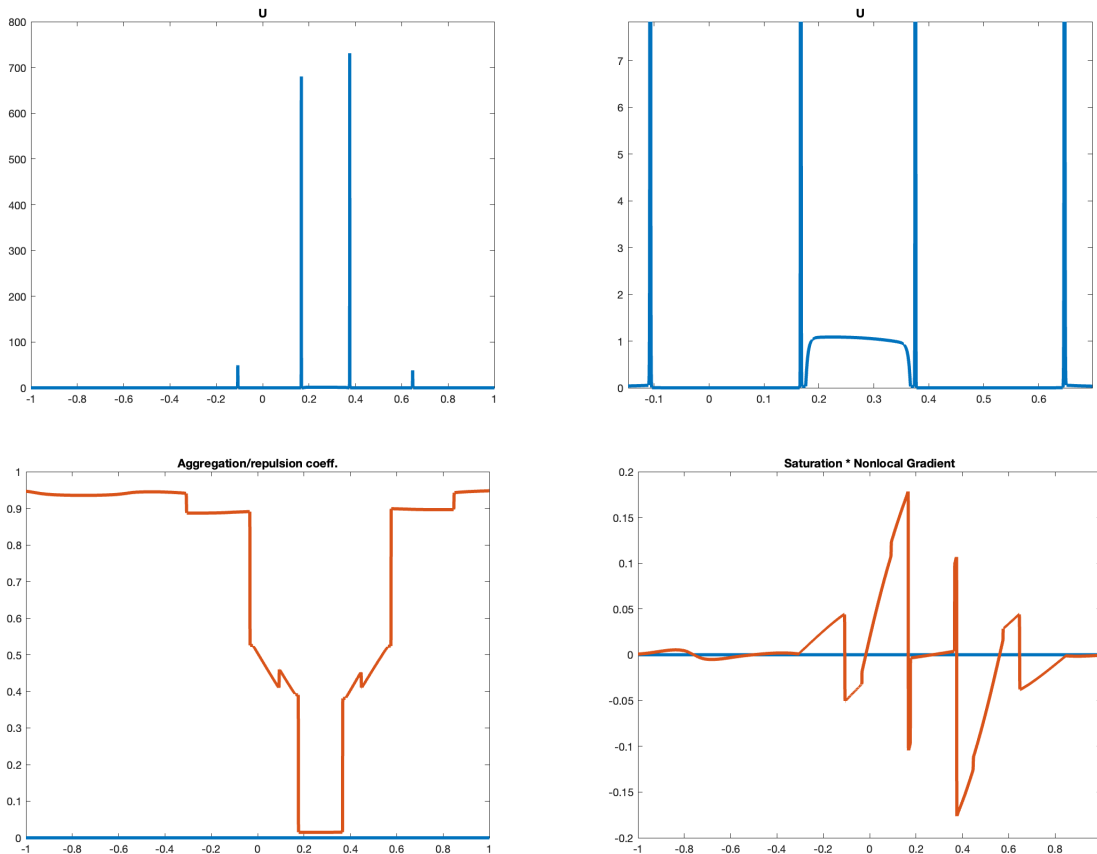


FIGURE 6. Evolution of a cell population under equilibrated nonlocal parameters $R = R_{sat} = 0.2$ governed by very strong aggregation ($K = 0.95$). On the first line we depict the cell distribution profile at the equilibria together with a zoom. As before the second line shows the pictures of the saturation coefficient and the flux term.

From now on, we consider a constant initial condition $u_0(x) = 1/2$, representing the fact that initially, cells are random distributed along the domain, and we follow its evolution according to model 3.14. In contrast to numerical experiments considering periodic conditions, in which constant initial conditions are perturbed in a tiny area to start the dynamics, in our case such perturbation is not needed. Isolated boundary conditions immediately act on the cells positioned at the boundaries, which are attracted towards the interior through the non local gradient, whenever the capacity is large enough. On the contrary, if capacity is small, cells will accumulate at the boundary as a result of repulsion. The parameters we choose in the following experiments for the nonlocal processes are $R = 0.5$, $R_{sat} = 0.1$ and now the appropriate interaction strength parameter is $\gamma = 10^4$. Note the strong reduction of the saturation radius in the following examples with respect to the previous simulations, whereas we have enlarged the sensing radius upto $R = 0.5$. The purpose of these choices is to contrast the resulting PDEs with the subsequent Lagrangian trajectories in the next section. Indeed, Figure 4.0.3 includes several examples with precisely fixed values $R = 0.5$ and $R_{sat} = 0.1$. We show that for large values of the nonlocal capacity K , cell distribute more uniformly through the interval, preventing accused accumulations. However, as long as the value of K grows, the dynamics resembles the APS strong aggregation model [2], shown in Figure 10.

The first example depicted in Figure 7 corresponds to a relatively strong aggregation dynamics, with capacity $K = 0.7$. In the initial stages two accumulation peaks appear close to the boundary, due to the sign of the nonlocal gradient near the boundary. Later on, the central remaining cells eventually aggregate in another accumulated peak. Due to the high aggregation/saturation coefficient K , repulsion does not take place. This fact can be observed in the second picture of Figure 7. Then, the motion is mainly driven by the increasing difference of population density balanced by the nonlocal gradient. It is multiplied by a positive saturation coefficient, thus it addresses the motion towards the accumulations, see the third picture of Figure 7. However, in the last zoomed pictures of Figure 7, we appreciate in the equilibria state a small diffusion effect. Indeed a zoom, for example on the left hand side peak, shows a thin area where there are still cells around that accumulation. We note that close to the strong aggregations the nonlocal gradient is almost null (because the balance performed within a $2R$ width is close to zero), hence along this narrow zone the diffusion, though weak, still disperses the cells. Accordingly, a zoom on the saturation coefficient reveals that it is slightly curved, as it can be appreciated in the last picture.

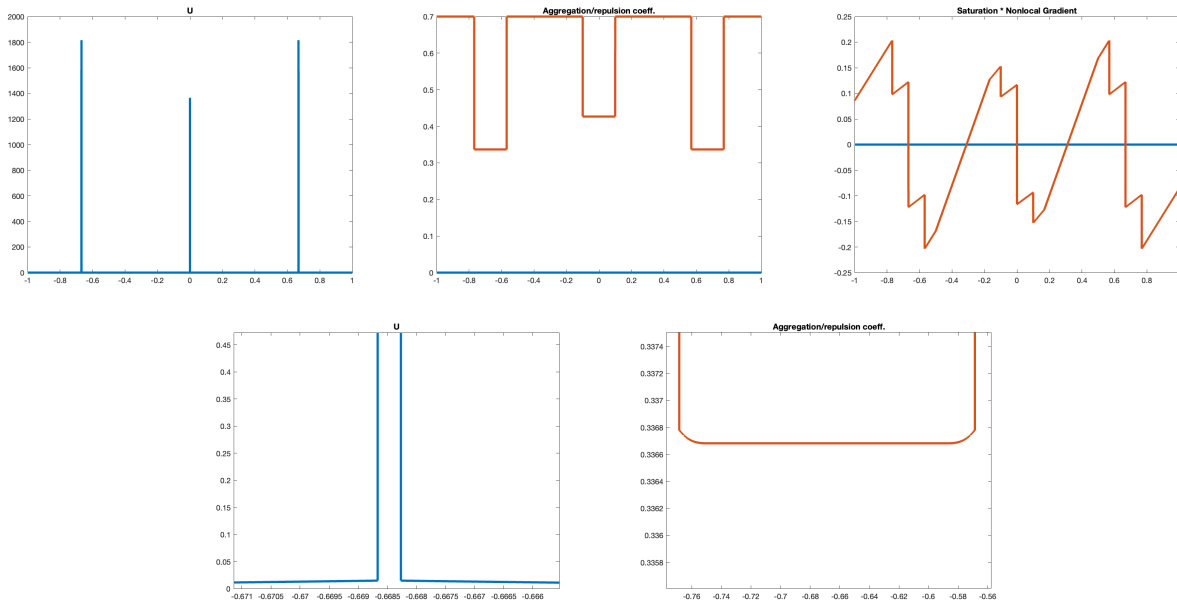


FIGURE 7. Simulations of model 3.14 from a constant initial condition $u_0(x) = 1/2$ and parameters $R = 0.5$, $R_{sat} = 0.1$ and $K = 0.7$. On the first line we represent the final distribution cell profile, the saturation/aggregation coefficient and the flux. On the second line we have performed a zoom of the final profile at the accumulation situated around $x \sim -0.6685$ on the right. The zoom on the left corresponds to the final graphic of the coefficient at the interval $[-0.78, -0.56]$.

The same experiment reducing the capacity coefficient up to $K = 0.3$, enlarges the repulsion, which is now present around $x = -0.7$ and $x = 0.7$. Now, the two previous accumulation peaks close to the boundary split into two. This final profile can be appreciated in Figure 8. Note in the last picture the slope of the interaction term at $x \sim -0.6$ and $x \sim 0.6$, that send cells to each of the two peaks. However, the central peak does not produce repulsion, see third picture, thus a unique aggregation remains. In the second picture we have performed a zoom on the left hand side of the equilibrium profile, to observe that there exists a dense region of cells around the aggregations, wider than in the example with capacity $K = 0.7$.

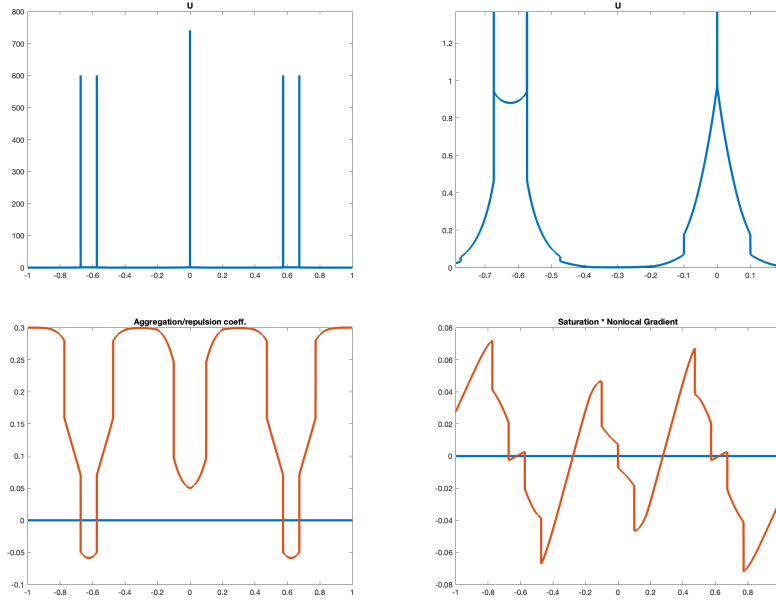


FIGURE 8. Simulations of model 3.14 from a constant initial condition $u_0(x) = 1/2$ and parameters $R = 0.5$, $R_{sat} = 0.1$ and $K = 0.3$. The first picture corresponds to the final density profile, where we have performed a zoom on the left hand side of the domain, to appreciate the existence of cells between the strong accumulations. On the second line we include the graphics of the aggregation/repulsion coefficient and the drift term at this final stage.

At the sight of the previous example we wonder if it is just the repulsion what prevents the higher accumulations observed in Figure 7, or if the diffusion also plays a role to form these dense areas. This originates the next simulation in Figure 9, in which take as initial condition the previous equilibria in Figure 8, under the same dynamics as before, but with different intensities for diffusion and interactions. Precisely, now we enlarge the previous interaction coefficient $\gamma = 10^4$ up to $\gamma = 10^5$. Figure 9 reveals that the diffusion still disperses the cells around the peaks, which have decreased their densities but still present. Again, in the zoom of the interaction term in last picture, we can appreciate the small role of the interactions around $x \sim -0.6$ (and similar for $x \sim 0.6$).

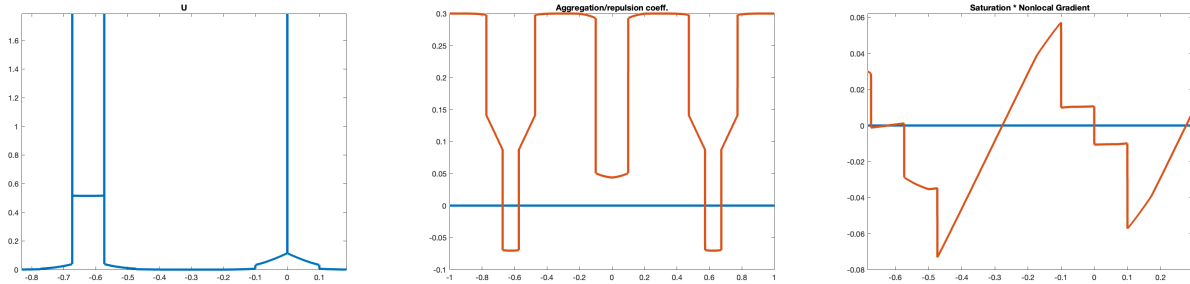


FIGURE 9. Simulations from the previous equilibrium profile in Figure 8 as initial condition and $\gamma = 10/h$. The first picture corresponds to a zoom of the final profile on the left hand side of the domain while the last picture is a zoom at the same left side of the drift term. The central picture shows the repulsion/aggregation coefficient on the whole domain.

4. LAGRANGIAN PERSPECTIVE

In this section agent based models are derived where the unknown variable is the position of the cells at certain time t , instead of its density. Let us start by considering a single population of N cells randomly distributed in a bounded unidimensional domain $[-L, L] \subset \mathbb{R}$, at initial positions $x_i(0)$, $i = 1, \dots, N$. We will select a particle at an arbitrary position $x_i(0)$ and follow its trajectory, $x_i(t)$, along the time, according to the different processes involved. The following system of stochastic differential equations describes how the position of each of the N cells evolves along time:

$$(4.1) \quad dx_i(t) = \frac{1}{N} \sum_{j \neq i} F(x_j(t), x_i(t)) dt + \sqrt{2\varepsilon} B_t^i, \quad i = 1, \dots, N, \quad t > 0.$$

Here, $F(x_j, x_i)$ represents the action of the particle j interfering on the trajectory of the particle i . In fact, we assume that $F(x_j, x_i) = F(|x_j - x_i|)$, where $|\cdot|$ denotes the Euclidean distance. In the so-called hydrodynamic limit (as $N \rightarrow \infty$) this fact will lead to obtain nonlocal terms in the resulting deterministic PDEs. The coefficient $1/N$ in (4.1) ensures that the interaction on particle i is of first order, so that mean field equations can be obtained. The term (B_t^i) , $i = 1, \dots, N$, $t \geq 0$ denotes independent standard Brownian motions on \mathbb{R} , which will drive the diffusion. Though the diffusion coefficient ε could depend on the position of the particle i or even on the positions of the global population, being decreasing with respect to the density of particles, it will be considered constant.

Systems as (4.1) are classic in many contexts in Physics, Biology, Economics, Sociology, etc., where it is necessary to analyze the motion of a large number of particles, and describe their positions and velocities, combining deterministic and stochastic processes. The existing literature in this field is infinite and it is increasing over time due to the interest aroused by its multiple and useful applications. For a general overview on this topic and specific applications to biological processes, such as population dynamics including logistic growth and repulsion effects, tumoral cell growth, among others even in finance and markets, we refer to the book [5] and references therein. For further references in stochastic equations with applications in swarming we refer to the Chapter [6], related to fluid mechanics, granular flows, traffic models, or large communications networks, see [3], and references included in these collections.

The identification of the underlying PDE from a discrete system of N stochastic differential equations as $N \rightarrow \infty$ is an intricate process requiring a strong knowledge of Probability Theory, which

undoubtedly has interest itself. However, our main objective in this Section is to have a complementary perspective to the Eulerian optics of the system. Whereas the previous approach has sense only for h (interval length) small in order to have a continuous density of cells, we can always consider a fewer number of cells and follow their trajectories along time. In this way we expect to extract more qualitative information and additional features from interactions, than with the former simulations. As counterpart, it could happen that saturation or repulsion effects could be not properly described when N is not large. Thus each perspective reveals complementary information with respect to the other.

Therefore, we connect the subsequent discrete interactions forces with the previous PDEs formally. For a short presentation, we follow the course notes collected in [4]. The empirical measure of the system of cells is given by

$$\mu_t^N = \frac{1}{N} \sum_{i=1}^N \delta_{x_i(t)},$$

where δ_x is the Dirac mass on $x \in \mathbb{R}$.

Let $\varphi : [-L, L] \rightarrow \mathbb{R}$ be an observable function and x_t a trajectory of a cell. How does $\varphi(x_t)$ evolves in time according to μ_t^N ? Recall Itô's formula

$$d\varphi(x_t) = \left[F(x, y) \frac{d\varphi}{dx} + \frac{\varepsilon^2}{2} \frac{d^2\varphi}{dx^2} \right] dt + \varepsilon \frac{d\varphi}{dx} dB_t.$$

Then, from (4.1), it holds for each i

$$\begin{aligned} \langle \varphi, \delta_{x_i(t)} \rangle - \langle \varphi, \delta_{x_i(0)} \rangle &= \varphi(x_i(t)) - \varphi(x_i(0)) = \int_0^t \left[\frac{1}{N} \sum_{j \neq i} F(x_i(s), x_j(s)) \frac{d\varphi}{dx}(x_i(s)) + \varepsilon^2 \frac{d^2\varphi}{dx^2}(x_i(s)) \right] ds \\ &\quad + \sqrt{2}\varepsilon \int_0^t \frac{d\varphi}{dx}(x_i(s)) dB_s^i. \end{aligned}$$

Furthermore, averaging in $(x_i)_{i=1}^N$, one has

$$\begin{aligned} \langle \varphi, \mu_t^N \rangle - \langle \varphi, \mu_0^N \rangle &= \int_0^t \frac{1}{N} \sum_{i=1}^N \left[\frac{1}{N} \sum_{j \neq i} F(x_i(s), x_j(s)) \frac{d\varphi}{dx}(x_i(s)) + \varepsilon^2 \frac{d^2\varphi}{dx^2}(x_i(s)) \right] ds \\ &\quad + \sqrt{2}\varepsilon \int_0^t \frac{1}{N} \sum_{i=1}^N \frac{d\varphi}{dx}(x_i(s)) dB_s^i \\ &= \int_0^t \int_{-L}^L \left[\int_{-L}^L F(x, y) d\mu_s^N(y) \frac{d\varphi}{dx}(x) + \varepsilon^2 \frac{d^2\varphi}{dx^2}(x) \right] d\mu_s^N(x) ds \\ &\quad + \sqrt{2}\varepsilon \int_0^t \frac{1}{N} \sum_{i=1}^N \frac{d\varphi}{dx}(x_i(s)) dB_s^i. \end{aligned}$$

It is well known that passing to the hydrodynamic limit there exists a measure μ_t such that $\mu_t^N \rightarrow \mu_t$ as $N \rightarrow \infty$, and

$$(4.2) \quad \int_{-L}^L \varphi d\mu_t - \int_{-L}^L \varphi d\mu_0 = \int_0^t \int_{-L}^L \left[\int_{-L}^L F(x, y) d\mu_s(y) \operatorname{div}_x \varphi + \varepsilon^2 \Delta \varphi(x) \right] d\mu_s(x) ds,$$

given that by the law of large numbers it holds that

$$\sqrt{2\varepsilon} \int_0^t \frac{1}{N} \sum_{i=1}^N \frac{d\varphi}{dx_i}(x_i(s)) dB_s^i \rightarrow 0, \quad \text{as } N \rightarrow \infty.$$

Notice that, in case that the measure μ_t is absolutely continuous with respect to the spatial variable, equation (4.2) represents the weak formulation of a general PDE of the form

$$u_t(x, t) = \varepsilon^2 u_{xx} - \partial_x \left(u(x, t) K(u)(x, t) \right),$$

where $K(u)(x, t)$ takes into account the balance of the forces exerted on the particles placed on x . After rescaling in time, we can rewrite it as

$$u_t(x, t) = u_{xx} - \gamma \partial_x \left(u(x, t) K(u)(x, t) \right),$$

where the parameter $\gamma > 0$ regulates the strength of the interactions with respect to the diffusion. Depending on the different interacting forces, we recover the PDEs (3.10), (3.13) and (3.14), now under the Lagrangian perspective.

The core of the following subsections is describing the effects of each discrete interacting force giving rise to the previous models. In the subsequent we have considered doubly isolated dynamics. Then, each of the previous PDEs are subjected to the boundary conditions (3.15).

4.0.1. Strong aggregation model [2].

Let us begin our analysis with the Lagrangian formulation of the APS model, which exhibits strong aggregation, by defining

$$(4.3) \quad \begin{aligned} \sum_{j \neq i} F(x_i, x_j) &= \gamma \sum_{j=1}^N w(|x_i - x_j|) \mathbb{1}_{0 < x_j - x_i < R} \mathbb{1}_{x_j \in [-L, L]} - \gamma \sum_{j=1}^N w(|x_i - x_j|) \mathbb{1}_{-R < x_j - x_i < 0} \mathbb{1}_{x_j \in [-L, L]} \\ &:= R_i - L_i \end{aligned}$$

The characteristic function $\mathbb{1}_{x_j \in [-L, L]}$ guarantees that the dynamics take place inside the domain. Notice that the cells with interior positions such that $|x_i \pm L| > R$ move according to the balance between the density of cells on their right and on their left, weighted by a positive function $w(r)$, which decreases linearly with respect to the distance $r = |x_i - x_j|$. However, as the cell is closer to the boundary, F is no longer a balance and it is more likely that the particle moves towards the interior. Note that at first stages, when the cells are still all spread, it is improbable that repulsion plays a role. This fact yields contractive dynamics except for the Brownian motion.

4.0.2. Local saturation coefficient [7].

Trajectories corresponding to this model are influenced by the following discrete interactions:

$$\sum_{j \neq i} F(x_i, x_j) = (R_i - L_i) \left(1 - \frac{1}{k} \frac{1}{N} \frac{1}{K(a, N)} \sum_{j=1}^N \mathbb{1}_{|x_j - x_i| < a} \right),$$

where R_i, L_i are declared in (4.3), $0 < k \leq 1$ represents the local crowding capacity and $K(a, N) \rightarrow 0$ and $a \rightarrow 0$ as $N \rightarrow \infty$.

4.0.3. A new nonlocal aggregation/repulsion coefficient.

In the spirit of avoiding large accumulations, we propose to take a nonlocal coefficient that regulates the transport, by setting

$$\sum_{j \neq i} F(x_i, x_j) = (R_i - L_i) \left(1 - \frac{1}{k} \frac{1}{N} \sum_{j=1}^N \widehat{\omega}(|x_j - x_i|) \mathbb{1}_{|x_j - x_i| < R_{sat}} \right),$$

with R_i, L_i defined in (4.3) and $R_{sat} > 0, 0 < k \leq 1$ are fixed constants. We can also ponder the importance of the distance between cells in the nonlocal aggregation/repulsion coefficient through the weight $\widehat{\omega}$, which could be linear decreasing with the distance or a positive constant.

4.1. Numerical Simulations.

Along this Section we include several numerical experiments illustrating the different dynamics exhibited by the previous discrete models. All of the simulations are performed for $N = 100$ cells interacting within the interval $[-L, L]$ with $L = 1$, run up to final time $T = 15$ with time step being $\Delta t = 0.001$.

Recall that the movement of any cell i follows the following structure

$$dx_i(t) = F(\vec{x})dt + \varepsilon^2 dB_i(t),$$

where $\varepsilon^2 > 0$ the diffusion coefficient is considered to be constant and precisely $\varepsilon^2 = 0.4$.

We approximate its movement by using finite differences in the deterministic term and sampling a Normal distribution to reproduce the Brownian motion. Namely,

$$(4.4) \quad x_i(t + \Delta t) = x_i(t) + \Delta t F(\vec{x}) + \varepsilon^2 N(0, \Delta t).$$

Note that the variance of the Gaussian is Δt , hence the jump is almost differential. Regarding the transport term, the sensitivity radius is chosen to be $R = 0.5$, where the interactions among cells are weighted inversely proportional to their distance as $\omega(r) = (R - r)/R$.

Strong aggregation: The whole population of cells converges to single points in absence of repulsion or saturation. Indeed, notice that those accumulation points do not interact among themselves since they lay outside of the sensitivity interval of the others. However, cells keep having small oscillations due to the Brownian Motion, almost unappreciated in Figure 10 for $\varepsilon^2 = 0.4$, which could be more perceptible as the diffusion coefficient ε grows.

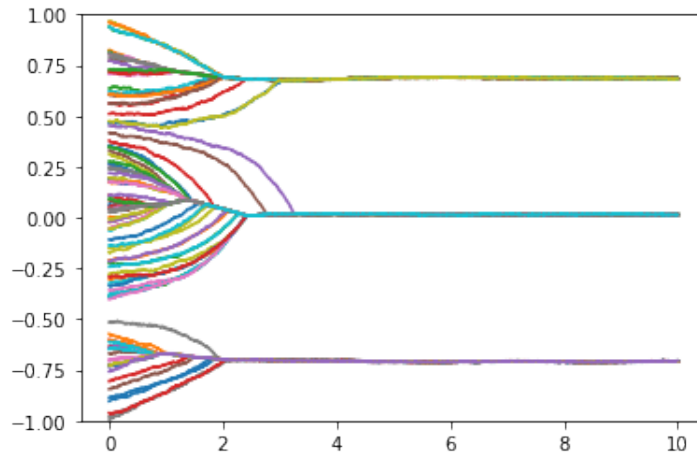


FIGURE 10. Evolution of the movement of 100 cells through time according to Model 4.0.1 with strong aggregation. The diffusion coefficient $\varepsilon^2 = 0.4$, the sensing radius $R = 0.5$ and the corresponding weight $\omega(r) = (R - r)/R$.

Local saturation coefficient. As suggested in [7], it is natural that the cells move towards high populated areas, since the probability of finding other cells is higher than in isolated areas. Thus, the authors assume that the transport term moves as in model 4.0.1. However, to avoid strong aggregation they consider a velocity coefficient given by $u(1 - u)$. Recall that in this reference $0 \leq u \leq 1$. Therefore, at populated areas where u is close to one, the velocity of motion becomes neglectful at these points. Adhesion/repulsion forces are taken depending on the distance between cells through the weight w .

Nevertheless, we would see more natural that repulsion effects were observed when passing certain prescribed threshold or capacity k . Having this in mind our first attempt is to propose as velocity coefficient the term $u(1 - u/k)$, for some $0 < k < 1$, see model 4.0.2. This choice will drive aggregation in low populated areas, until eventually the local capacity threshold k might be reached and then repulsion starts to play its role. In the discrete formulation it will be necessary to introduce then the parameters $a = 1/N$ and $K(a, N) = 2a$, which approach to the term $(1 - u/k)$ for N large.

As observed in Figure 11, this population also evolves towards several wide tubes. Though they could interact one with each other, they do not approximate due to the repulsion produced by the term $(1 - u/k)$. On the other hand, an aggregation effect (weaker than in model 4.0.1) makes that the cells remain in continuous motion within the tubes. This fact is a consequence of the irregularity of the velocity coefficient $(1 - u/k)$, whose values change extremely rapidly from positive to negatives values and conversely.

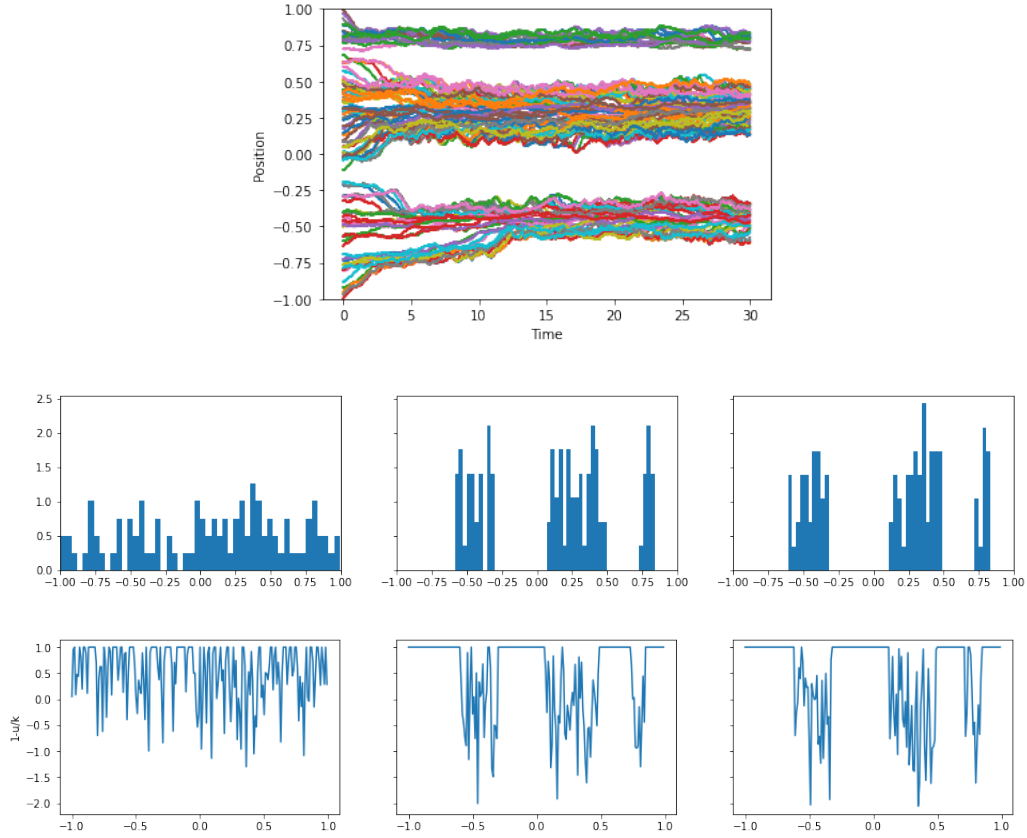


FIGURE 11. Position of 100 cells evolving according to Model 4.0.2 is depicted, and the corresponding histograms at times $t = 0$, $t = T/2$ and $t = T = 15$. Finally, the plot of the discrete approximation of the velocity coefficient $1 - u/k$ for $k = 0.3$ at times $t = 0$, $t = T/2$ and $t = T = 15$ is included.

In view of these simulations we propose to compute the velocity of the cells motion, not locally at each position x through the term $(1 - u/k)$, but in an interval around that position, $[x - R_{sat}, x + R_{sat}]$. This is precisely model 4.0.3.

Nonlocal aggregation/repulsion coefficient: Tubes are also formed in a similar fashion of the previous model. The difference is that now in model 4.0.3 the capacity is not measured locally. Cells look at an interval of radius R_{sat} from their position and they may move towards or away from the high concentration of cells. This feature induces stronger aggregation than in model 4.0.2. On the other hand, now the nonlocality of the velocity coefficient regularizes its values, as can be appreciated in Figures 12 and 13, where $R_{sat} = 0.1$ and nonlocal capacity $k = 0.3$ (independent on N).

Furthermore, the weight in the nonlocal coefficient is taken constant in both examples, namely $\hat{\omega} \equiv 1$, given that $R_{sat} \ll R$ to appreciated distance effects. However, depending on the weight function ω involved in the nonlocal gradient, the cells can distribute uniformly along the tubes, as in Figure 12, where $\omega(y) = (R - y)/R$. In contrast, for the choice $\omega(y) \equiv 1$ their aggregation is weaker and accumulated on the boundary of such tubes, as Figure 13 shows.

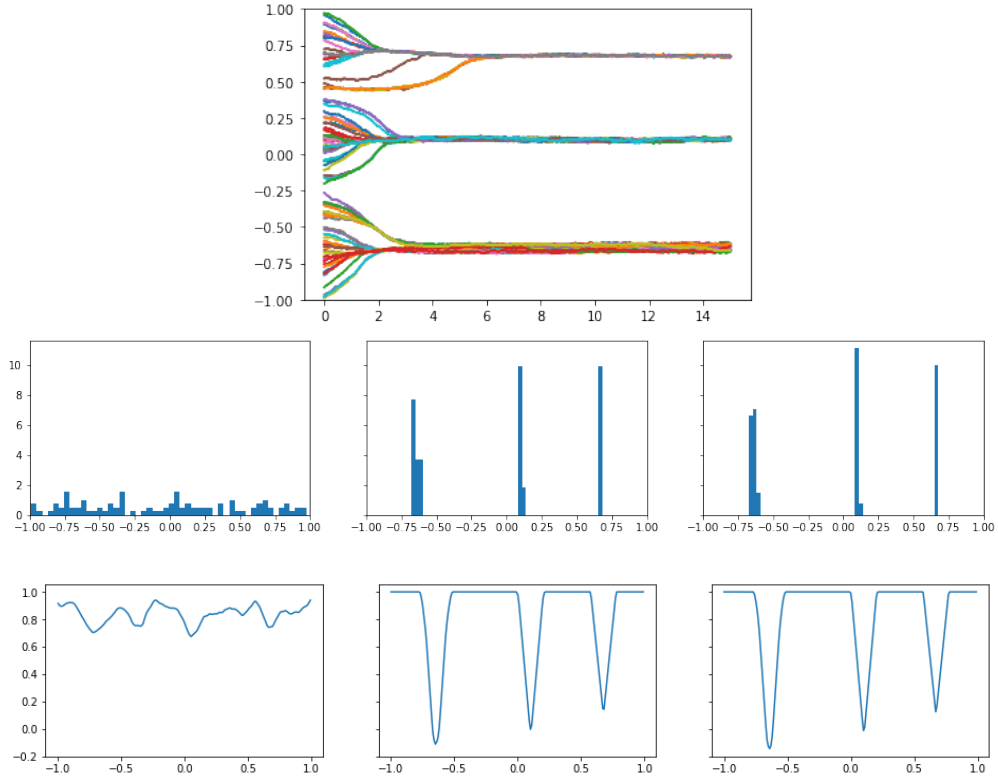


FIGURE 12. Evolution of 100 cells over time in Model 4.0.3 and linear weight ω and saturation weight $\hat{\omega} \equiv 1$. The saturation radius $R_{sat} = 0.1$ and nonlocal capacity $k = 0.3$. Below, the corresponding histograms and the plot of the discrete approximation of the velocity coefficient $1 - \frac{1}{k} \int_{x-R_{sat}}^{x+R_{sat}} u(y) dy$ at times $t = 0$, $t = T/2$ and $t = T = 15$ are depicted.

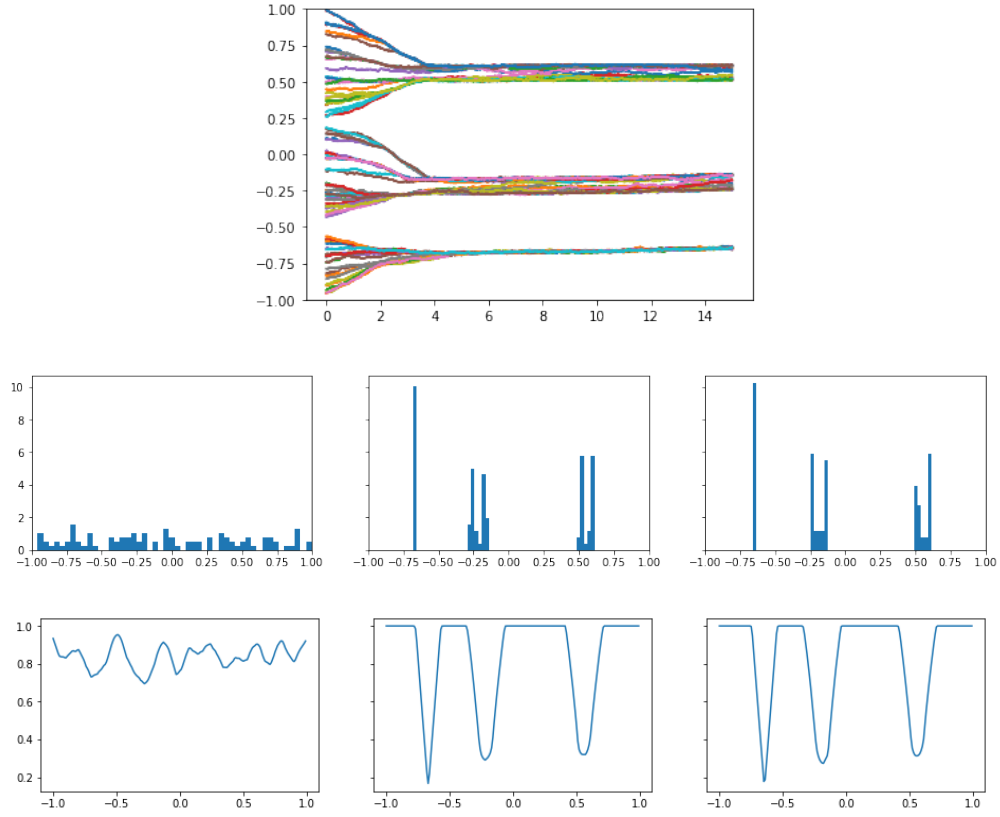


FIGURE 13. Evolution of 100 cells over time in Model 4.0.3 with both weights, $\omega \equiv 1$ and $\hat{\omega} \equiv 1$. The rest of the parameters are exactly the same as in Figure 12

Role of capacity with local diffusion: We conclude our simulations by exploring further the role of the capacity regarding the strength of the aggregation. We compare the effect exerted by different values of the capacity parameter k on models 4.0.2 and 4.0.3. Obviously, higher values of capacity yield stronger aggregation in both cases. However, while in model 4.0.2 the continuous motion of cells (due to the rapidly change of sign of the local velocity coefficient), prevents to recover the asymptotic strong aggregation model 4.0.1 when $k \nearrow 1$, model 4.0.3 resembles strong aggregation for $k = 0.7$. See Figures 14 and 15. We also stress that the dynamics for $k = 0.3$ and linear weight $\hat{\omega}$ in Figure 12 is similar to the dynamics appreciated in Figure 15 with the same capacity $k = 0.3$ but constant weight $\hat{\omega} \equiv 1$. Finally, we would like to remark the correspondence of Figure 15 for $k = 0.7$ with Figure 7 under the PDE approach. Moreover, enlarging the repulsion we can appreciate in Figure 8 that the accumulations closer to the boundaries split each into two with a remaining populated zone between each peak. This resembles to Figure 15 with $k = 0.3$, where tubes are wider representing the fact that cells move within the accumulation area.

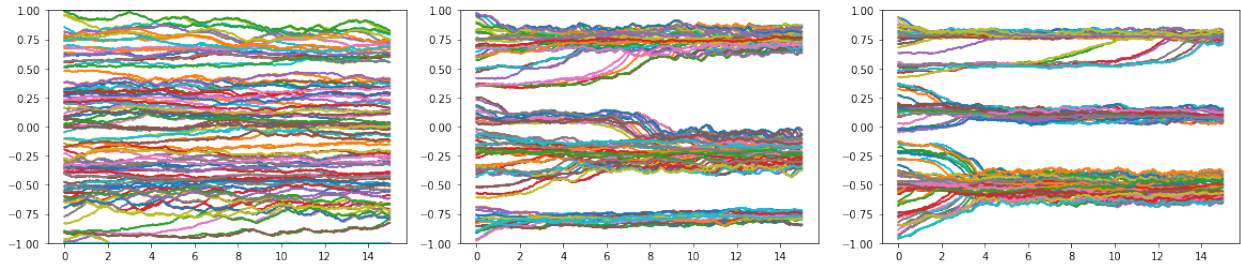


FIGURE 14. Model 4.0.2 for lineal weight $\omega(y) = (R - y)/R$ and values $k = 0.2$, $k = 0.5$ and $k = 0.7$, respectively.

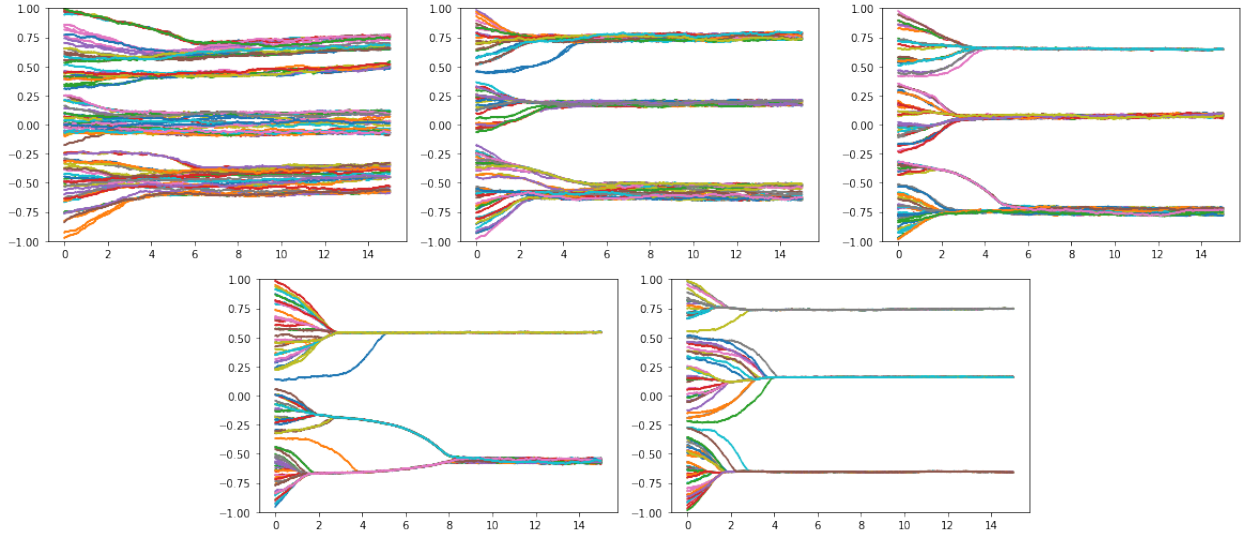


FIGURE 15. Model 4.0.3 with lineal weights $\omega(y) = (R - y)/R$, $\hat{\omega}(y) = (R_{sat} - y)/R_{sat}$ and values $k = 0.1$, $k = 0.2$, $k = 0.3$, $k = 0.5$ and $k = 0.7$, respectively.

5. CONCLUSIONS

The main goal achieved in this work is the modelling of large single populations of cells under different interactions among themselves, in balance with their diffusive motion. One of our starting points is the well known contribution due to Armstrong–Painter–Sherratt [2], which drives cell motion towards the most populated areas through a drift term in the direction of certain nonlocal gradient, yielding very strong aggregation. We also pay attention to [7], where these high accumulations at single points are softened by adding a local saturation coefficient, slowing down the motion at points where the density attains large values.

A review of those mentioned previous works is performed, focusing on one single population cell-cell adhesion dynamics. The underlying PDEs are deduced from diverse discrete problems, assembling the individual motion of each cell as a result of the competing diffusion and interacting rules. These discrete relations are settled under two different perspectives: Eulerian (how many particles arrive to certain position?) and Lagrangian (if a particle is situated initially at certain position x , how is its trajectory along the time?). These complementary points of view, yielding of course the same PDEs, are helpful to understand deeply the models included in [2] and [7], when the diffusion is given by the Laplacian.

At this point, a new model with respect to the ones in [2] and [7] is proposed, including repulsion from too saturated areas as part of the drift term. We notice that this makes a difference from the mentioned articles. Recall that [2] does not consider repulsion. In [7] this repulsion effect is described as diffusive mechanism, considering a porous media diffusion operator in the PDE. The authors also suggest to use changing sign weights in the definition of the nonlocal gradient. However, the sign is chosen according to the distance between the interacting cells, but not as a result from saturation in crowded areas. Our proposal includes a coefficient inside the drift term, accounting for the density of cells in a neighbourhood of each of them. If its value does not exceed a prescribed capacity threshold, the particle moves towards most populated zones. But as soon as this neighborhood density goes beyond the threshold capacity, the particle is immediately repulsed in the opposite direction, towards least populated areas. Moreover, choosing the threshold capacity close to one, and a small value for the saturation radius, no repulsion takes place and simulations resemble the original strong aggregation dynamics in [2].

In addition, the nonlocal gradient is weighted by a nonnegative function being linear decreasing with respect to the distance between the interacting cells. This choice distributes more uniformly the cells inside the aggregation tubes, than using a constant weight as in [2] and [7], which gives the same importance to long or short range interactions within the sensing radius.

On the other hand, we remark that in the models proposed in [2] and [7] periodic boundary conditions are considered, as approach of the fact that the size of the domain is infinitely large with respect to the cell size. However, this simplification is not appropriate to model dynamics in very small or thin tubes, as it could happen to describe some in vitro experiments. Alternatively, we propose confining the dynamics inside the domain preserving the mass under the assumption that no particles enter or leave the domain. For simplicity, in our simulations we examine the particular case of double isolation: Homogeneous Neumann boundary conditions for the diffusion, and null nonlocal gradient at the boundary, for the interactions.

We show that taking constant initial data, representing the fact that the cells are initially uniformly distributed along the domain, the dynamics begins precisely at the boundaries. The isolated conditions drive the cells positioned close to the boundaries towards the interior, as a result of attraction, whenever the capacity threshold is large enough. Conversely, they are pushed to the boundaries, under strong repulsion. In any case, this first motion at the boundaries, produced exclusively by the isolation conditions (diffusion and drift term are null for constant solutions), permits that now diffusion and drift terms act, starting the whole dynamics. This is an important difference with respect to periodic boundary conditions, for which a perturbation of constant initial data is needed to give rise to some dynamics. Moreover, this observation matches with the fact that some cells are motile only in confined environments.

Acknowledgements: This research was initially conducted while CGF visited University of Seville thanks to the Feder project entitled *Diferentes Perspectivas para Modelos Biomatemáticos: Modelización, Análisis y Aproximación* (US-1381261), of reference 2021/00001597.

REFERENCES

1. K. Anguige and C. Schmeiser, *A one-dimensional model of cell diffusion and aggregation, incorporating volume filling and cell-to-cell adhesion*, J. Math. Biol. **58** (2009), no. 3, 395–427. MR 2470195
2. N. J. Armstrong, K. J. Painter, and J. A. Sherratt, *A continuum approach to modelling cell adhesion*, Journal of theoretical biology **243** (2006), no. 1, 98–113.

3. N. Bellomo and M. Pulvirenti, *Generalized kinetic models in applied sciences*, Modeling in applied sciences, Model. Simul. Sci. Eng. Technol., Birkhäuser Boston, Boston, MA, 2000, pp. 1–19. MR 1763150
4. F. Bolley, *Limite de champ moyen de systèmes de particules*, Séminaire: Equations aux Dérivées Partielles. 2009–2010, Sémin. Équ. Dériv. Partielles, École Polytech., Palaiseau, 2012, pp. Exp. No. XXXI, 15. MR 3098635
5. V. Capasso and D. Bakstein, *An introduction to continuous-time stochastic processes*, third ed., Modeling and Simulation in Science, Engineering and Technology, Birkhäuser/Springer, New York, 2015, Theory, models, and applications to finance, biology, and medicine. MR 3362672
6. J. A. Carrillo, M. Fornasier, G. Toscani, and F. Vecil, *Particle, kinetic, and hydrodynamic models of swarming*, Mathematical modeling of collective behavior in socio-economic and life sciences, Model. Simul. Sci. Eng. Technol., Birkhäuser Boston, Boston, MA, 2010, pp. 297–336. MR 2744704
7. J. A. Carrillo, H. Murakawa, M. Sato, H. Togashi, and O. Trush, *A population dynamics model of cell-cell adhesion incorporating population pressure and density saturation*, J. Theoret. Biol. **474** (2019), 14–24. MR 3948738
8. L. Chen, K. Painter, C. Surulescu, and A. Zhigun, *Mathematical models for cell migration: a non-local perspective*, Philosophical Transactions of the Royal Society B: Biological Sciences **375** (2020), no. 1807, 20190379.
9. M. Fritz, *Tumor evolution models of phase-field type with nonlocal effects and angiogenesis*, Bull. Math. Biol. **85** (2023), no. 6, Paper No. 44, 34. MR 4578408
10. V. Giunta, T. Hillen, M. Lewis, and J. R. Potts, *Local and global existence for nonlocal multispecies advection-diffusion models*, SIAM J. Appl. Dyn. Syst. **21** (2022), no. 3, 1686–1708. MR 4447423
11. R.J. Hawkins, M. Piel, G. Faure-Andre, A. M. Lennon-Dumenil, J. F. Joanny, J. Prost, and R. Voituriez, *Pushing off the walls: A mechanism of cell motility in confinement*, Phys. Rev. Lett. **102** (2009), 058103.
12. N. Loy and L. Preziosi, *Modelling physical limits of migration by a kinetic model with non-local sensing*, J. Math. Biol. **80** (2020), no. 6, 1759–1801. MR 4096763
13. H. Murakawa and H. Togashi, *Continuous models for cell-cell adhesion*, Journal of Theoretical Biology **374** (2015), 1–12.
14. J. P. Pinasco, V. Semeshenko, and P. Balenzuela, *Modeling opinion dynamics: theoretical analysis and continuous approximation*, Chaos Solitons Fractals **98** (2017), 210–215. MR 3632850
15. E. Rocca, L. Scarpa, and A. Signori, *Parameter identification for nonlocal phase field models for tumor growth via optimal control and asymptotic analysis*, Math. Models Methods Appl. Sci. **31** (2021), no. 13, 2643–2694. MR 4365199

CARLO GIAMBIAGI FERRARI, FRANCISCO GUILLÉN-GONZÁLEZ, MAYTE PÉREZ-LLANOS AND ANTONIO SUÁREZ
DEPARTAMENTO DE ECUACIONES DIFERENCIALES Y ANÁLISIS NUMÉRICO
FACULTAD DE MATEMÁTICAS, U. DE SEVILLA, C. TÁRFA, S/N, 41012 SEVILLA, SPAIN
Email address: cgf@gmail.com, guillen@us.es, mpperez@us.es, suarez@us.es